



UDP-sugar substrates of HAS3 regulate its O-GlcNAcylation, intracellular traffic, extracellular shedding and correlate with melanoma progression

Ashik Jawahar Deen¹ · Uma Thanigai Arasu¹ · Sanna Pasonen-Seppänen¹ · Antti Hassinen⁴ · Piia Takabe¹ · Sara Wojciechowski³ · Riikka Kärnä¹ · Kirsi Rilla¹ · Sakari Kellokumpu⁴ · Raija Tammi¹ · Markku Tammi¹ · Sanna Oikari^{1,2}

Received: 25 November 2015 / Revised: 25 January 2016 / Accepted: 4 February 2016 / Published online: 16 February 2016
© Springer International Publishing 2016

Abstract Hyaluronan content is a powerful prognostic factor in many cancer types, but the molecular basis of its synthesis in cancer still remains unclear. Hyaluronan synthesis requires the transport of hyaluronan synthases (HAS1-3) from Golgi to plasma membrane (PM), where the enzymes are activated. For the very first time, the present study demonstrated a rapid recycling of HAS3 between PM and endosomes, controlled by the cytosolic levels of the HAS substrates UDP-GlcUA and UDP-GlcNAc. Depletion of UDP-GlcNAc or UDP-GlcUA shifted the balance towards HAS3 endocytosis, and inhibition of hyaluronan synthesis. In contrast, UDP-GlcNAc surplus suppressed endocytosis and lysosomal decay of HAS3, favoring its retention in PM, stimulating hyaluronan synthesis, and HAS3 shedding in extracellular vesicles. The concentration of UDP-GlcNAc also controlled the level of O-GlcNAc modification of HAS3. Increasing O-GlcNAcylation

reproduced the effects of UDP-GlcNAc surplus on HAS3 trafficking, while its suppression showed the opposite effects, indicating that O-GlcNAc signaling is associated to UDP-GlcNAc supply. Importantly, a similar correlation existed between the expression of GFAT1 (the rate limiting enzyme in UDP-GlcNAc synthesis) and hyaluronan content in early and deep human melanomas, suggesting the association of UDP-sugar metabolism in initiation of melanomagenesis. In general, changes in glucose metabolism, realized through UDP-sugar contents and O-GlcNAc signaling, are important in HAS3 trafficking, hyaluronan synthesis, and correlates with melanoma progression.

Keywords 4MU · Mannose · Glucosamine · GNPDA · UGDH · OGT

Introduction

Hyaluronan is a non-sulfated linear glycosaminoglycan made up of repeating –GlcUA β 1,3–GlcNAc β 1,4– disaccharide units. It is secreted by many animal cell types, and is involved in various cellular functions like proliferation, adhesion, migration, and apoptosis—processes associated to multiple aspects of normal cell and tissue physiology [9, 37, 40, 52, 55]. Hyaluronan can adopt multiple roles depending on its content, location, size (fragmentation) and the type of cells synthesizing it [47, 50], and is particularly important in inflammation [12, 18] and cancer [41, 49]. Hyaluronan is synthesized in plasma membrane by a family of hyaluronan synthases (HAS1-3), utilizing cytosolic UDP-glucuronic acid (UDP-GlcUA) and UDP-*N*-acetyl glucosamine (UDP-GlcNAc) as substrates, and is simultaneously extruded into the extracellular space [57]. HASs are normally active only when present in plasma

Electronic supplementary material The online version of this article (doi:10.1007/s00018-016-2158-5) contains supplementary material, which is available to authorized users.

✉ Ashik Jawahar Deen
ashik.jawahardeen@uef.fi

✉ Sanna Oikari
sanna.oikari@uef.fi

¹ Institute of Biomedicine, School of Medicine, University of Eastern Finland, 70210 Kuopio, Finland

² Institute of Dentistry, School of Medicine, University of Eastern Finland, 70210 Kuopio, Finland

³ A. I. Virtanen Institute for Molecular Sciences, School of Medicine, University of Eastern Finland, 70210 Kuopio, Finland

⁴ Faculty of Biochemistry and Molecular Medicine, University of Oulu, 90014 Oulu, Finland

membrane [36], and are strongly dependent on the cytosolic concentrations of UDP-GlcNAc and UDP-GlcUA [19, 33]. Therefore, these two factors, the supply of UDP-sugars, and the transport of HAS to plasma membrane, are crucially important for the rate of hyaluronan synthesis. Indeed, the only known chemical agents specifically inhibiting HAS activity work by limiting the availability of UDP-GlcUA [28] or UDP-GlcNAc [19]. Accordingly, experimental augmentation of the UDP-sugar contents enhances hyaluronan synthesis [19]. The depletion of UDP-GlcUA is achieved by 4-methyl umbelliferone (4MU), the facile glucuronidation of which leads to a rapid depletion of the cellular UDP-GlcUA pool [21, 23]. Feeding cells with high concentrations of mannose reduces cellular UDP-GlcNAc content. The target of mannose influence appears to be glucosamine-6-phosphate deaminase (GNPDA), an enzyme that can either deplete or increase the most important intermediate (glucosamine-6-phosphate) in the UDP-GlcNAc synthesis pathway [6, 19]. UDP-GlcNAc and to some extent UDP-GlcUA is increased by feeding cells with glucosamine [19, 54]. It enters the cells through glucose transporters, and is directly phosphorylated to glucosamine-6-phosphate, thus bypassing the rate-limiting step in UDP-GlcNAc biosynthesis, catalyzed by the enzymes glutamine fructose-6-phosphate amidotransferase (GFAT) and GNPDA. Suppression of the UDP-sugar supply can also be accomplished by knockdown of key enzymes in their biosynthesis pathway, i.e. GFAT and GNPDA for UDP-GlcNAc, and UDP-glucose-6-dehydrogenase (UGDH) for UDP-GlcUA. An illustration of the UDP-sugar biosynthesis pathways, and its interference by chemicals, and by siRNA suppression of enzymes, are shown in Fig. 1.

While it is obvious that UDP-sugars have a strong impact on hyaluronan synthesis, it is not only due to a direct effect as a substrate in the enzymatic reaction. Published reports have shown that alterations of UDP-sugar levels by treating cells with 4-methyl umbelliferone (4MU), mannose and glucosamine also change the transcriptional activity of HAS2 gene [20, 53] and the turnover of HAS2 protein [54]. Our recent work showed that the vesicular traffic to/from plasma membrane is highly important for HAS3 enzymatic activity, since blocking the reverse traffic of HAS3 from plasma membrane to endosomes by Rab10 siRNA increased HAS3 level in plasma membrane, and hyaluronan synthesis as a consequence [8]. Nothing is known about the interplay between UDP-sugar supply and HAS transport to plasma membrane, while there is indirect evidence suggesting that the trafficking of HAS is integrated with the metabolism of UDP-sugars [36].

Hyaluronan synthesis has turned out to be a crucial determinant in carcinogenesis [48] and cancer progression [41, 46]. However, while knowledge of the molecular basis

of hyaluronan influences on cell behavior has accumulated during the years [46, 51], the ways of hyaluronan synthesis activation in cancer have remained obscure. A particular puzzle has been that increased *HAS* gene expression has not been reported in many cancers with elevated levels of hyaluronan [29, 30]. We therefore hypothesized that post-translational effects are involved, and that the enhanced glucose uptake in many cancers due to aerobic glycolysis [56], could increase the metabolic flux of glucose to UDP-sugars, and thus influence hyaluronan synthesis, as schematically presented in Fig. 1. This work showed that hyaluronan synthesis was affected especially by UDP-GlcNAc, which (1) acts as an immediate precursor in hyaluronan synthesis, (2) increases the O-GlcNAc modification of HAS3 protein, (3) controls HAS3 lysosomal degradation and (4) increases HAS3 residence time in plasma membrane. UDP-sugars could thus have a major influence on hyaluronan synthesis in malignant tumors, as suggested by analysis of human skin melanomas.

Materials and methods

Cell culture

MV3 and C8161, human melanoma cell lines and COS1, a monkey fibroblast-like kidney cell line were cultured in Dulbecco's minimal essential medium with high glucose (4500 mg/l) (Euroclone, Milan, Italy), 10 % fetal bovine serum (FBS) (Hyclone, Logan, UT, USA), 4 mM L-glutamine (Sigma), 50 µg/ml streptomycin sulfate, and 50 units/ml penicillin (Sigma). HEMA, a human primary melanocyte cell line (Thermo Scientific) was cultured in MGM-4 growth medium with the supplements (MGM-4 BulletKit, Lonza), as directed by the manufacturers.

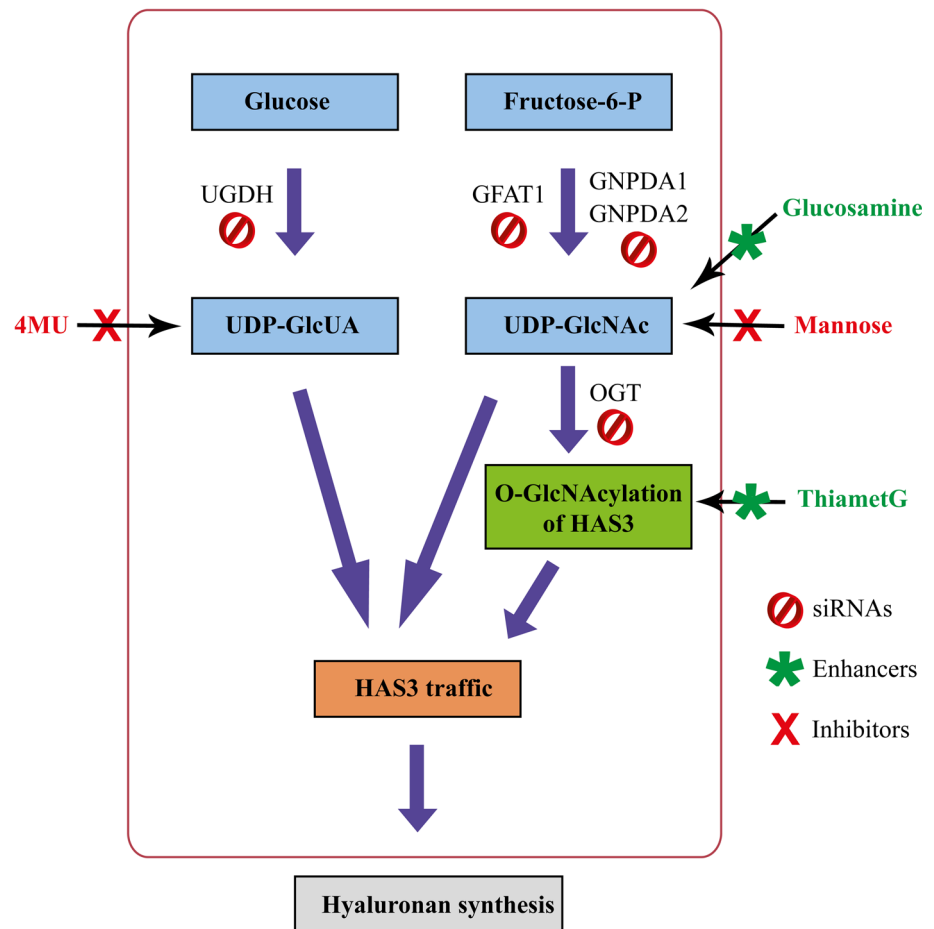
MV3 cells with EGFP-HAS3 overexpression

The MV3 cells stably overexpressing doxycycline-inducible EGFP-HAS3 [45] were sorted by FACS following induction to obtain a homogenous population with optimal EGFP fluorescence and maintained in 50 µg/ml hygromycin.

Treatments

Mannose was used at 20 mM final concentration, 4MU at 0.5 mM, glucosamine at 0.5–2.0 mM, and ThiametG at 20 µM, all from Sigma. The treatments were for 6 h at 37 °C in 2.5 % FBS unless indicated otherwise. Pericellular hyaluronan was removed with 1 TRU/ml of *Streptomyces* hyaluronidase (Seikagaku Co, Tokyo, Japan), added to medium 0.5–1 h before analysis.

Fig. 1 Schematic illustration of the synthesis of UDP-sugars and their influence on HAS3, its traffic, and hyaluronan synthesis. The target sites of the chemical agents: 4-methylumbelliferone (4MU), mannose and glucosamine, known to modify hyaluronan synthesis by reducing or enhancing the levels of UDP-sugars, are indicated. Likewise, the key enzymes in UDP-sugar biosynthesis, UDP-glucose-6-dehydrogenase (UGDH), glucosamine-6-phosphate deaminase 1 and 2 (GNPDA1, GNPDA2), and glutamine fructose-6-phosphate aminotransferase 1 (GFAT1), subjected to siRNA-mediated depletion to reduce UDP-sugars, are also shown. Additionally, O-GlcNAcylation of HAS3, enhanced by ThiametG and reduced by knockdown of O-GlcNAc transferase (OGT), is presented



Materials

EGFP-HAS3 and Dendra2-HAS3 plasmids, expressing human HAS3, were described previously [33, 35]. Rabbit polyclonal anti-EEA1 (Cell Signaling, Danvers, MA, USA), rabbit polyclonal anti-GFP (Invitrogen, Life Technologies Ltd, Paisley, UK), goat polyclonal anti-rabbit and anti-mouse Dylight 680 (Thermo Scientific), mouse monoclonal RL2 anti-O-GlcNAc (ab2739, Abcam, Cambridge, UK), Rabbit anti-Actin (Sigma), Mouse monoclonal anti-golgin 97 (Cell Signaling), Mouse monoclonal anti-CD44 (Hermes 3; gift from Prof. Sirpa Jalkanen, University of Turku, Finland), Rabbit polyclonal anti-GFAT1 (Catalog No: 14132-1-AP, Protein Tech, Chicago, IL 60612, USA) and Texas red-labelled anti-rabbit antibodies (Vector Laboratories, CA, USA) were also used. TurboFect (Thermo Scientific) was used for plasmid transfection. For confocal and TIRF imaging, cells were grown in eight-well μ -slides (ibiTreat, ibidi, GmbH, 82152 Planegg/Martinsried, Germany). For TIRF, the glass bottom slides were coated with rat tail type I collagen (BD Biosciences). Dynabeads[®] Protein G, Dynabeads[®] M-280 Streptavidin,

EZ-Link[™] Sulfo-NHS-SS-Biotin, and Deep mask red plasma membrane stain were purchased from Invitrogen (Life technologies). MTT (3-(4,5-dimethylthiazol-2-yl)-2,5-diphenyltetrazolium bromide) was purchased from Sigma.

SiRNA transfection

SiRNAs against GFAT1 (40 nM), GNPDA1 + 2 (25 nM each), UGDH (40 nM) and OGT (40 nM) were from Eurogentec (Seraing, Belgium), scrambled (control) siRNA (40 nM) from Origene (Rockville, MD, USA), and pre-designed siRNA against CD44 (30 nM) from Ambion (Thermo Scientific) (Table 1). SiRNAs were transfected using Lipofectamine RNAiMAX (Invitrogen). The media with the siRNAs were removed 6 h later and replaced with medium containing 2.5 % serum. 24 h later, EGFP-HAS3 was induced with 0.05 μ g/ml doxycycline, and 48 h post-siRNA transfection the cells were used for experiments. The primers used for analyzing specific genes are listed in Table 2. The silencing efficiencies (~50–90 %) are shown in Suppl. Figure 1A.

Table 1 Sequences of siRNA oligonucleotides used in this study

siRNA	Sequence (5′–3′)
Scrambled (control)	Origene (ref no: SR30004)
GFAT1 (NM_002056.2)	GAGGAAGAGUCAACUUUGA (sense) UCAAAGUUGACUCUCCUC (antisense)
GNPDA1 (NM_005471.4)	GAGAGGUGAUGAUCCUUAU (sense) AUAAGGAUCAUCACCUCUC (antisense)
GNPDA2 (NM_138335.1)	CGGGAAUGCUGCAGAUUUA (sense) UAAAUCUGCAGCAUCCCCG (antisense)
UGDH (NM_003359.3)	GGACACUGGUGAUACAAGA (sense) UCUUGUAUCACCAGUGUCC (antisense)
OGT (NM_181672.2)	GCCAAGGCAUGUUAUUUGA (sense) UCAAAUAACAUGCCUUGGC (antisense)
CD44 (NM_000610.3)	Ambion (catalog no: 16708A)

Table 2 Sequences of Q-PCR primers used in this study

Q-PCR primers	Sequence (5′–3′)
RPLPO (NM_001002.3)	For: AGATGCAGCAGATCCGCAT Rev: GTGGTGATACCTAAAGCCTG
GFAT1 (NM_002056.2)	For: GGATATGATTCTGCTGGTGTG Rev: CCAACGGGTATGAGCTATTC
GNPDA1 (NM_005471.4)	For: GACCTTCAACATGGATGAGT Rev: TGTGGGTGTTTTCTGGGT
GNPDA2 (NM_138335.1)	For: TTTGTATGCGATGAAGATGC Rev: TGAATTTTGTCCAGTCTCC
UGDH (NM_003359.3)	For: TCTGTTGCATCGGTGCAGGCT Rev: TCAGATCTGCTGCCCGGCT
OGT (NM_181672.2)	For: GCTGAGAGGCACGGCAACCT Rev: ACACGCAGCCGACCATCACT
CD44 (NM_000610.3)	For: CATCTACCCAGCAACCCTA Rev: CTGTCTGTGCTGTCCGGTGAT

HPLC analysis of UDP-sugars

250,000 MV3-EGFP-HAS3 cells were plated in six-well plates, transfected with the siRNAs and induced with 0.05 µg/ml doxycycline for 24 h. Treatments with 4MU, mannose, glucosamine, and ThiametG were for 6 h. Cells were then scraped off in PBS, sonicated, and analyzed for UDP-sugars as previously described [31].

Confocal microscopy and live cell imaging

Fluorescent 512 × 512 pixel images were taken with 40× (NA 1.3) and 63× (NA 1.4) oil objectives on a Zeiss Axio

Observer equipped with a Zeiss LSM 700 confocal module (Carl Zeiss Microimaging) and a Zeiss XL-LSM S1 incubator with temperature and CO₂ control. DRAQ5 nuclear staining (2 µM, Biostatus Ltd., Leicestershire, UK) was used to evaluate the transfection efficiency.

Analysis of HAS3 traffic

For the analysis of forward traffic, MV3 parental cells transfected with Dendra2-HAS3 plasmids were treated with the chemical modifiers or siRNAs. Just before imaging a Deep mask red indicator was added, and a region of interest (ROI) was drawn around PM. A second ROI was drawn around the perinuclear region, corresponding to Golgi, and a 405 nm laser pulse (10 % laser power, 10 iterations for 1 s) was applied there to convert part of the green Dendra2-HAS3 to red. The red intensities of the two ROIs were tracked for 1 h with 10 min intervals. The red fluorescence at PM ROI in each time point was divided by the fluorescence of the PM dye, and expressed as fold change of time point “0”. The disappearance of red HAS3 from the peri-nuclear ROI was measured in the same way.

For retrograde traffic, photoconversion of Dendra2-HAS3 was done in ROI drawn with the PM marker as reference, images of this ROI were collected at 2 min intervals for 16 min, and results expressed as for anterograde traffic.

Imaging HAS3 by total internal reflection fluorescence (TIRF) microscope

A Zeiss cell observer spinning disc confocal microscope with a 100× oil objective (NA 1.46) and a TIRF unit was used for 488 nm excitation of EGFP-HAS3 vesicles in the cytoplasmic side of plasma membrane in MV3 cells. Images were collected at 0.5 s intervals for 2 min and analyzed with ImageJ program. Using a 25 arbitrary units threshold value and a ROI to exclude background and Golgi area, the number of EGFP-positive vesicles was counted in each time point and normalized to the initial number of vesicles. Based on the fold change of vesicle numbers in each time point, a linear regression (“trend”) line was calculated and from the equation ($y = mx + c$) standard deviation (SD) for each time point was calculated as follows: $SD = (\text{actual value} - \text{theoretical value of vesicle number})$, where theoretical value of vesicle number = $(m \times \text{vesicle number in the 'nth' time point}) + c$. The mean SD value for each treatment, representing the fluctuation of the number of vesicles, was calculated and expressed as fold change to control.

Analysis of HAS3 degradation

Dendra2-HAS3 was photoconverted in the whole cell and the disappearance of red HAS3 was analyzed for 5 h at

20 min intervals. DIC images were used to correct for possible drift in optical focus.

Analysis of HAS3-positive extracellular vesicles

5000 MV3-EGFP-HAS3 cells suspended in 150 μ l of a collagen mix (2.9 mg/ml of type I collagen in EBSS with 0.1 % acetic acid, 0.24 % of sodium bicarbonate, and 21 mM sodium hydroxide) were plated in a eight-well μ -slide and incubated for 1 h at 37 °C. Culture medium was added on top of the solidified matrix and 24 h later EGFP-HAS3 expression was induced for 24 h. The cells were fixed with 4 % paraformaldehyde in 100 mM phosphate buffer (PB) and immunostained for CD44 (1:250 in 1 % BSA-PB). Confocal 1028 \times 1028 pixel images were taken as stacks of optical sections of 1 μ m thickness with a 63 \times objective and compressed into a single image. EGFP-HAS3-positive extracellular vesicles were counted using ImageJ and normalized to cell numbers in the field.

Cell lysis and analysis of HAS3 O-GlcNAcylation

MV3-EGFP-HAS3 cells were plated in T75 culture flasks, treated with siRNAs (scrambled, OGTi) as described above and induced with 0.25 μ g/ml doxycycline for 24 h. Later in some of the groups, cells were treated with or without chemical mediators (control, 20 mM mannose, 1 mM glucosamine and 20 μ M ThiametG) for 6 h. Additionally, MV3 cells were also transiently transfected with EGFP and grown for 24 h. All the steps in cell lysis, described below, were done in ice-cold condition or +4 °C (centrifugation). The cells were scraped and pelleted in 1 \times phosphate buffered saline (PBS), washed thrice in PBS, lysed in 1 ml of Tris-Triton X buffer pH 7.8 [25 mM Tris, 150 mM NaCl, 1 mM CaCl₂, 0.1 % SDS, 0.5 % Triton X-100 with 1:200 protease inhibitor cocktail (Sigma)] by sonication, and spun down at 1000 and 2500 rpm to remove any intact cells and nuclear debris, respectively. The resulting supernatant was saved and protein concentration in the lysate was measured using BCA kit (Pierce, Thermo Scientific). 1 μ g of anti-GFP antibody was conjugated to 25 μ l of Dynabeads[®] Protein G magnetic beads and EGFP-HAS3 from 1 mg of lysate was immunoprecipitated according to manufacturer's instructions. In case of EGFP immunoprecipitation, the GFP antibody was first conjugated to the magnetic beads with 2.5 mM BS3 crosslinker (Thermo Scientific) prior addition of lysate. The immunoprecipitated EGFP-HAS3 was eluted using 20 μ l of 4 \times SDS sample buffer and in case of EGFP, elution was done with 15 μ l of 0.1 M glycine-HCl (pH 3.0), followed by immediate addition of 5 μ l of 1 M Tris-0.5 M NaCl (pH 8.0) and 7 μ l of 4 \times SDS sample buffer. The immunoprecipitated fractions were boiled at 65 °C for 15 min and tested for

O-GlcNAcylation using RL2 anti-O-GlcNAc antibody in western blot.

Biotinylation of cell surface HAS3 and recycling assay

COS1 cells at 50–70 % confluency in T75 culture flasks were transfected with EGFP-HAS3. The cultures were treated with control and OGT siRNAs for 48 h and with 4MU, mannose, glucosamine and ThiametG for 6 h in fresh 2.5 % FBS media. Recycling of EGFP-HAS3 in plasma membrane was studied as described [44], with minor modifications. Culture dishes on ice were washed with ice-cold PBS and incubated with 1 mM of freshly prepared EZTM-link Sulfo-NHS-SS-biotin in PBS for 30 min and washed thrice with ice-cold PBS. Unreacted biotin was quenched with 50 mM Tris in ice-cold PBS for 10 min and washed thrice with ice-cold PBS. To allow internalization of biotinylated EGFP-HAS3, the cells were incubated at 37 °C for 30 min and then cell surface biotin was cleaved with 100 mM DTT in ice-cold PBS for 15 min, preceded and followed by three ice-cold PBS washes. Then incubation was continued at 37 °C for 30 or 60 min, which brought intracellular biotinylated EGFP-HAS3 back to plasma membrane. The DTT-treatment was repeated and cell lysates were prepared. EGFP-HAS3 was immunoprecipitated by an EGFP antibody with the final elution using 30 μ l of 0.1 M glycine-HCl (pH 3.0), followed by immediate addition of 5 μ l of 1 M Tris-0.5 M NaCl (pH 8.0) and resuspension in 1 ml of ice-cold PBS. A second immunoprecipitation was performed with 75 μ l of Dynabeads[®] M-280 Streptavidin magnetic beads, as per the manufacturer's instructions. Biotinylated EGFP-HAS3 was eluted with 4 \times SDS sample buffer, heated at 65 °C for 15 min and western blotted for EGFP detection.

Western blotting

Immunoprecipitated EGFP-HAS3 and EGFP samples were subjected to 10 % SDS-PAGE and the proteins were transferred to nitrocellulose membranes (Protran, Whatman), blocked with 3 % bovine serum albumin (BSA) in Tris buffered saline containing 0.1 % Tween 20 (TBST) or 5 % skimmed milk-TBST for 1 h at room temperature and then incubated overnight with anti-GFP (1:2000, in 1 % BSA-TBST) or RL2 anti-O-GlcNAc (1:2000, in 3 % skimmed milk-TBST) or anti-Actin (1:2500, in 1 % BSA-TBST) antibodies. The blots were then washed thrice with TBST and incubated with anti-rabbit Dylight 680 (1:5000, in 1 % BSA-TBST) or anti-mouse Dylight 680 (1:5000, in 2 % milk-TBST) antibodies for 1 h at room temperature, and washed thrice with TBST. The stained blots were then imaged using LI-COR Odyssey Infrared imaging system (LI-COR Biosciences, Lincoln, NE, USA).

Hyaluronan assay

80,000 cells/well of MV3-EGFP-HAS3 cells were plated in 12-well plates, transfected with siRNAs (scrambled, GFATi, GNPDAi, UGDHi and OGTi) and induced with 0.05 µg/ml doxycycline for 24 h before collection of media. Culture medium was also collected after 24 h treatment with 4MU, mannose and glucosamine, and after 6 h treatment with ThiametG. When the incubations were terminated, cells were lysed in 250 µl of ice-cold Tris-Triton X buffer with 1:200 protease inhibitor cocktail (Sigma) by sonication and protein estimation was done. In some cases, cell numbers were also counted. The culture media were stored at -20 °C before hyaluronan (HA) assay by an enzyme-linked sorbent assay [14]. The results were calculated as HA (in ng) per total protein (in µg) and expressed as fold change to control or control siRNA. In some cases results were expressed as HA (ng)/10000 cells.

Immunofluorescence and early endosome antigen 1 (EEA1) staining

20,000 cells/well of MV3 were grown in eight-well µ-slides and transiently transfected with EGFP-HAS3 for 24 h. In some cases, after transfection, cells were treated with 1 TRU/ml of *Streptomyces* hyaluronidase for 1 h at 37 °C to remove the pericellular coat of hyaluronan. Cells were then fixed with 4 % paraformaldehyde in 0.1 M sodium phosphate buffer, pH 7.4 (PB) for 15–20 min and washed five times with PB. 10 min incubation at room temperature (RT) with 0.1 % Triton X-100 in 1 % bovine serum albumin (BSA) was used for permeabilization, and 20 min incubation at RT with 1 % BSA in PB for blocking. The cells were incubated with anti-EEA1 antibody (1:100 in 1 % BSA in PB), overnight, washed five times with PB and stained with Texas red-labelled anti-rabbit secondary antibody (1:500 in PB) for 1 h. After washing the stained cells, the plates were stored at 4 °C until use.

Cell proliferation assay

2500 cells/well of MV3-EGFP-HAS3 cells were plated in 96-well plates and treated with siRNAs and chemical mediators, as explained before. Later, 2.5 % growth media with 0.05 µg/ml doxycycline was replaced on a daily basis for 1–3 days. In groups with chemical mediators, the respective chemicals were also supplied along with doxycycline. Cells were then fixed, washed and permeabilized as above, and stained with 2 µg/ml of DAPI (4',6-diamidino-2-phenylindole) in PB for 15 min at 37 °C, and washed two times with PB. The nuclear DAPI fluorescence was measured in a plate reader equipped with a UV laser

and 355/460 nm excitation/emission filters (Victor multi-label plate reader, Perkin Elmer).

Cell adhesion to type I collagen

Cell adhesion assay to type I collagen, described previously [8], was followed with slight modifications. Briefly, MV3-EGFP-HAS3 cells were induced with 0.1 µg/ml doxycycline for 24 h, with the cells treated with siRNA transfection and chemical mediators, as described before. These cells were trypsinized and applied as 40,000/well in 96-well plates pre-coated with 0.25 mg/ml of type I collagen (BD Biosciences) using a medium containing 10 µg/ml of cycloheximide and no phenol red. After 30 min the unattached cells were washed away, the wells were incubated with 0.5 mg/ml of MTT in phenol-free medium for 2 h at 37 °C, and the incubation continued in DMSO for 5–10 min with gentle shaking. Absorbance values were measured at 540 and 620 nm (the latter for background). The results were calculated as absorbance values at 540 minus absorbance at 620 nm and expressed as fold change to control or control siRNA.

Cell migration assay

MV3-EGFP-HAS3 cells were plated as 160,000 cells/well in 12-well plates, and induced with 0.05 µg/ml doxycycline for 24 h. A scratch wound was introduced in the growth area in the wells using a pipette tip and the media in the wells were replaced with the ones containing chemicals (Control, 4MU, mannose and glucosamine) and doxycycline. The wound closure before (0 h) and after 24 h was imaged and analyzed using ImageJ. The wound closure area of 24 h images was normalized to that of 0 h and the results were expressed as fold change to control.

Image analysis

ZEN 2012 (grey), ZEN 2012 (blue) and ImageJ programs were used to analyze confocal microscopy images. Adobe Photoshop elements 11 and Adobe illustrator were used for presentation of the images. Images were brightness/contrast adjusted and, in some cases, non-linear adjustment was applied, all done uniformly across the control and treated groups to better visualize the cellular features of interest.

Tissue samples

Paraffin-embedded diagnostic tissue samples included benign nevi ($n = 8$), dysplastic nevi ($n = 9$), in situ melanomas ($n = 8$), superficial melanomas ($n = 7$, Breslow <1 mm) and deep melanomas ($n = 9$, Breslow >4 mm).

The Ethics committees of Kuopio University Hospital and The Finnish National Supervisory Authority for Welfare and Health (VALVIRA) have approved the study protocol.

Immunohistological staining of GFAT1 and evaluation

After deparaffinization, sections were boiled in 10 mM citrate buffer (pH 6.0) in a pressure cooker for 15 min and washed with 0.1 M phosphate buffer (PB; pH 7.0), kept in 1 % H₂O₂ for 5 min, washed, blocked with 2 % BSA in PB for 30 min at 37 °C, and incubated with the GFAT1 antibody (1:100) in 1 % BSA in PB overnight at 4 °C. After rinsing with PB, biotinylated anti-rabbit secondary antibody (1:300, Vector Laboratories, Irvine, CA, USA) in PB with 1 % BSA was added for 1 h at room temperature. After washes, visualization was done with avidin–biotin–peroxidase (1:200, Vector Laboratories,) and 0.05 % DAB (Sigma) and Mayer's hematoxylin counterstaining. Hyaluronan staining was done as described previously [39]. The intensities of the staining were estimated as follows; negative (0), weak (1), moderate (2) or strong (3).

Statistical analysis

Statistical analyses were done in GraphPad Prism 5.0 for Windows. One-way ANOVA with Tukey's post hoc test and Student's *t* test were used, with a *p* value <0.05 considered significant.

Results

Manipulation of cellular UDP-GlcNAc and UDP-GlcUA content influences hyaluronan synthesis

The MV3 melanoma cell cultures with inducible expression of EGFP-HAS3 (control) showed ~twofold increase in the cellular content of UDP-GlcNAc, when compared to uninduced cells (Fig. 2a). However, a ~50 % reduction in the cellular content of UDP-GlcNAc was seen in MV3 cells with EGFP-HAS3 expression, when treated with the previously established optimum concentration (20 mM) of mannose [19] (Fig. 2a). 4MU, known to deplete UDP-GlcUA [16], tended to reduce also UDP-GlcNAc [23] (Fig. 2a). Accordingly, silencing of UDP-GlcUA biosynthesis by UGDH siRNA showed a similar effect on UDP-GlcNAc (Fig. 2c), indicating that there is a connection between the productions of the two UDP-sugars. About 50 % reduction of UDP-GlcNAc was also obtained by siRNA for GFAT1, considered as a rate-limiting enzyme in the biosynthesis of UDP-GlcNAc (GFAT2 was not expressed in these cells). The siRNAs against the two

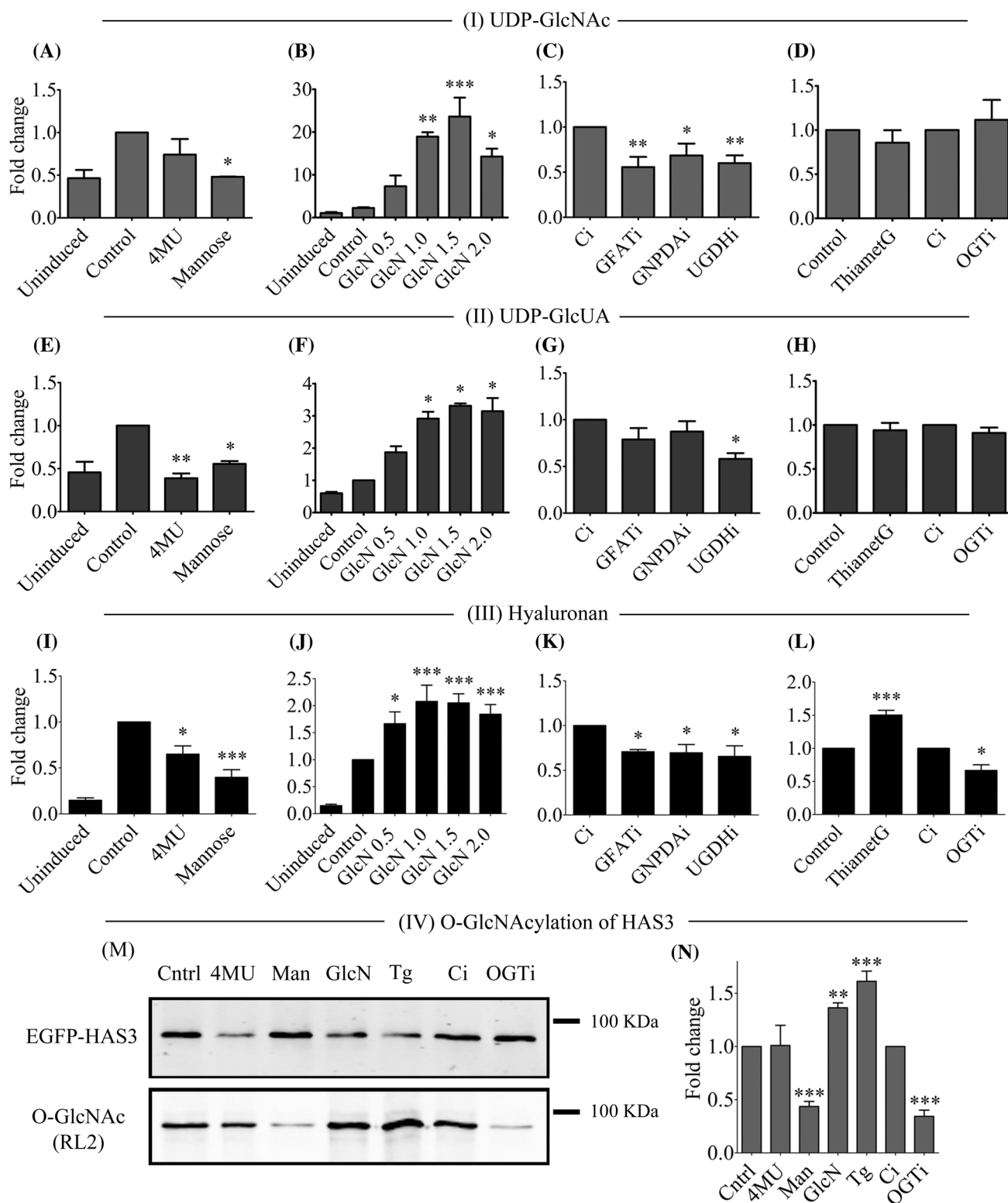
GNPDAs also reduced UDP-GlcNAc (Fig. 2c), a finding suggesting that they also contribute to the biosynthesis of UDP-GlcNAc. Glucosamine is taken up by the cells and phosphorylated to glucosamine-6-phosphate, thus bypassing the rate-limiting GFAT/GNPDA step, and resulting in a marked increase of cellular UDP-GlcNAc. The maximum increase (19–24-fold) was reached with 1.0–1.5 mM glucosamine (Fig. 2b). Thus, changes ranging ~0.5–20 times of control level were obtained in the cellular concentration of UDP-GlcNAc.

Similar to the cellular UDP-GlcNAc content, EGFP-HAS3 expression increased UDP-GlcUA by ~twofold when compared to uninduced cells (Fig. 2e). With the commonly used 0.5 mM concentration of 4MU, the content of UDP-GlcUA decreased to ~40 % of the control level (Fig. 2e). UDP-GlcUA was also decreased by siRNA against UGDH, the enzyme responsible for its synthesis (Fig. 2g). On the other hand, mannose, supposed to target mainly UDP-GlcNAc, decreased also UDP-GlcUA (Fig. 2e) and a tendency to reduction of UDP-GlcUA was also seen with siRNAs against GFAT1 (Fig. 2g), offering additional evidence for a coupling between the contents of the two UDP-sugars. Furthermore, addition of glucosamine increased also the content of UDP-GlcUA, although markedly less than UDP-GlcNAc (Fig. 2f). In summary, with these manipulations depletion of UDP-GlcUA down to 0.4 times of control was obtained, while ~threefold upregulation was obtained by glucosamine.

The induced EGFP-HAS3 expression dominated hyaluronan synthesis over that of the endogenous hyaluronan production in uninduced MV3-HAS3 cells (Fig. 2i). The observed effects on hyaluronan synthesis thus reflect changes that take place post-transcriptionally. The data showed that 4MU and mannose both reduced hyaluronan secretion, correlating with the depletion of the UDP-sugar substrates (Fig. 2i). Also, knockdown of GFAT1, both GNPDAs, and UGDH showed reduced hyaluronan secretion (Fig. 2k). Glucosamine, on the other hand, increased hyaluronan secretion, which peaked at 1.0–1.5 mM concentration, corresponding to the highest cellular contents of UDP-GlcNAc and UDP-GlcUA (Fig. 2j). Overall, the data show that UDP-sugars, acting as the building blocks for hyaluronan synthesis, strongly control hyaluronan synthesis at post-transcriptional level.

O-GlcNAc modification of HAS3 and regulation of hyaluronan synthesis

Besides a building block for the construction of hyaluronan, UDP-GlcNAc serves as a substrate for the dynamic regulation of protein functions by O-GlcNAcylation. We first studied whether the contents of the cellular UDP-sugars were affected by inhibition of enzymes that add (O-



GlcNAc transferase, OGT) and remove (O-GlcNAcase, OGA) O-GlcNAc moiety in the proteins. SiRNA silencing of OGT is supposed to reduce O-GlcNAcylation, while ThiametG, an inhibitor of OGA, is expected to move the

dynamic equilibrium of O-GlcNAcylation towards higher substitution levels. As shown in (Fig. 2d, h), interference in the activity of these enzymes did not influence the cellular content of the UDP-sugars. However, the synthesis of

Fig. 2 UDP-sugar levels influence hyaluronan synthesis and O-GlcNAcylation of HAS3. MV3-HAS3 cells induced for 24 h with 0.05 µg/ml doxycycline to overexpress EGFP-HAS3 were assayed for UDP-sugars, hyaluronan and O-GlcNAcylation. These dox-induced MV3-HAS3 cells otherwise untreated were used as controls. MV3-HAS3 cells without induction of EGFP-HAS3 (uninduced) were used as negative controls for the effect of induction. The siRNAs (GFAT1, GNPDA1, UGDH1, OGT1 and C1, the control siRNA) were introduced at the time of induction. The concentrations were normalized to total cell protein. (I) Fold changes in the concentration of UDP-GlcNAc compared to induced cultures (control, set as 1.0) are indicated. **a–d** 4-Methylumbelliferone (4MU), mannose (Man), glucosamine (GlcN), and ThiametG (Tg) were added at 0.5 mM, 20 mM, 0.5–2.0 mM, and 20 µM final concentrations, respectively, 6 h before analysis. (II) The concentrations of UDP-GlcUA in cells subjected to treatments as above, shown in **e–h**. (III) Hyaluronan in the growth medium was assayed after 24 h treatments, except the effect of ThiametG which was assayed after a 6 h treatment, as shown in **i–l**. (IV) O-GlcNAcylation of HAS3: MV3-HAS3 cells induced with 0.1 µg/ml doxycycline for 24 h and treated as for the UDP-sugar assays. Cell homogenates were immunoprecipitated with an anti-EGFP-antibody and divided in two identical samples, which were blotted and probed with antibodies against EGFP and O-GlcNAc, shown in **m**. The level of HAS3 O-GlcNAcylation was quantitated by the fluorescence ratio of O-GlcNAc to total EGFP, shown in **n**. The data represent mean ± SEM from 3–4 independent experiments. * $p < 0.05$, ** $p < 0.01$, *** $p < 0.001$ (one-way ANOVA, Tukey's test)

hyaluronan was significantly increased and decreased with higher and lower O-GlcNAcylation, respectively (Fig. 2l). These effects were similar to those obtained by manipulation of the UDP-GlcNAc, but since they took place without changes in UDP-GlcNAc, O-GlcNAcylation could be involved in the effects of UDP-GlcNAc content. We therefore studied whether HAS3 contains this modification, and whether it is affected by the fluctuation of the cellular UDP-GlcNAc content. Western blots of immunoprecipitated EGFP-HAS3 with an antibody against the O-GlcNAc moiety showed a signal that responded to increasing (Fig. 2m, n: GlcN) and decreasing UDP-GlcNAc contents (Fig. 2m, n: Man). Inhibition of OGA by ThiametG (Fig. 2m, n: Tg) enhanced HAS3 O-GlcNAcylation, while OGT knockdown suppressed it (Fig. 2m, n: OGT1). There was no response to decreasing UDP-GlcUA content (Fig. 2m, n: 4MU), and plain EGFP was not modified (Suppl. Figure 1B), supporting the specificity of the signal. Dynamic changes in cellular UDP-GlcNAc level thus influenced HAS3 O-GlcNAcylation, which is likely to account for the changed hyaluronan synthesis.

Photo-converted Dendra2-HAS3 as a tracer for the traffic between Golgi and cell surface

Our hypothesis was that UDP-sugar contents associate with the vesicular traffic and plasma membrane abundance of HAS3, with consequent changes in hyaluronan synthesis. This traffic was analyzed in MV3 cells by transfection of

Dendra2-HAS3, which can be photoconverted from green to red in specific subcellular sites, followed by time-lapse series to locate and quantify its subsequent movements. Dendra2-HAS3 in the perinuclear region was colocalized with the Golgi marker—golgin 97—confirming that these HAS3 deposits were in Golgi (Suppl. Figure 1C). A part of Dendra2-HAS3 also colocalized with the Deep Mask Red plasma membrane marker (Suppl. Figure 2A).

Untreated control cultures showed relatively slow disappearance of HAS3 from Golgi, its half-life exceeding 1 h (Suppl. Figure 2B). The increase in plasma membrane of HAS3, photoactivated in Golgi, was also slow during the 1 h observation time (Suppl. Figure 2C). The effects of UDP-sugar depletion and surplus, and changing the level of O-GlcNAcylation, were rather unexpected as all treatments tended to increase HAS3 outflow from Golgi, and reduce its appearance in cell surface. The result suggests that there is a large amount of stored HAS3 in Golgi, only a small part of which is normally mobilized towards plasma membrane. The data also suggest that control of this traffic is complex and may even involve recycling back to Golgi area. Moreover, the apparently slow overall flow of Dendra2-HAS3 from Golgi to cell surface, compared to the relatively faster endocytosis (Fig. 3), suggests that it is difficult to specifically determine the Golgi to cell surface flux rate of HAS3.

Control of HAS3 endocytosis by UDP-sugars

As a next step, the kinetics of photoconverted HAS3 moving away from cell surface was assayed (Fig. 3a). Deep Mask Red dye was used as a plasma membrane marker in MV3 cells and the corresponding region of interest (white line) was chosen to photo-convert Dendra2-HAS3 present in plasma membrane (Fig. 3a). The signal of photo-converted Dendra2-HAS3 (pseudo-colored as white, Fig. 3a, “Post” panels) in plasma membrane was measured over a time frame of 16 min with an interval of 2 min between the images and the trafficking kinetics was analyzed (Fig. 3b). This retrograde traffic (endocytosis) of HAS3 from plasma membrane was analyzed following the same treatments used above to modulate the UDP-sugar contents and O-GlcNAcylation in MV3 cells. As compared to control, HAS3 endocytosis rate in 4MU- and mannose-treated cells was significantly increased (Fig. 3b). In contrast, 2 mM glucosamine strongly inhibited HAS3 endocytosis. Reduction of the UDP-GlcNAc and UDP-GlcUA levels by silencing of GFAT1, GNPDAs, and UGDH resulted in an increased endocytosis of HAS3, similar to the effects of 4MU and mannose. Whether O-GlcNAcylation is involved in the cell surface retention of HAS3 was checked by increasing and decreasing O-GlcNAcylation by ThiametG and OGT siRNA. They

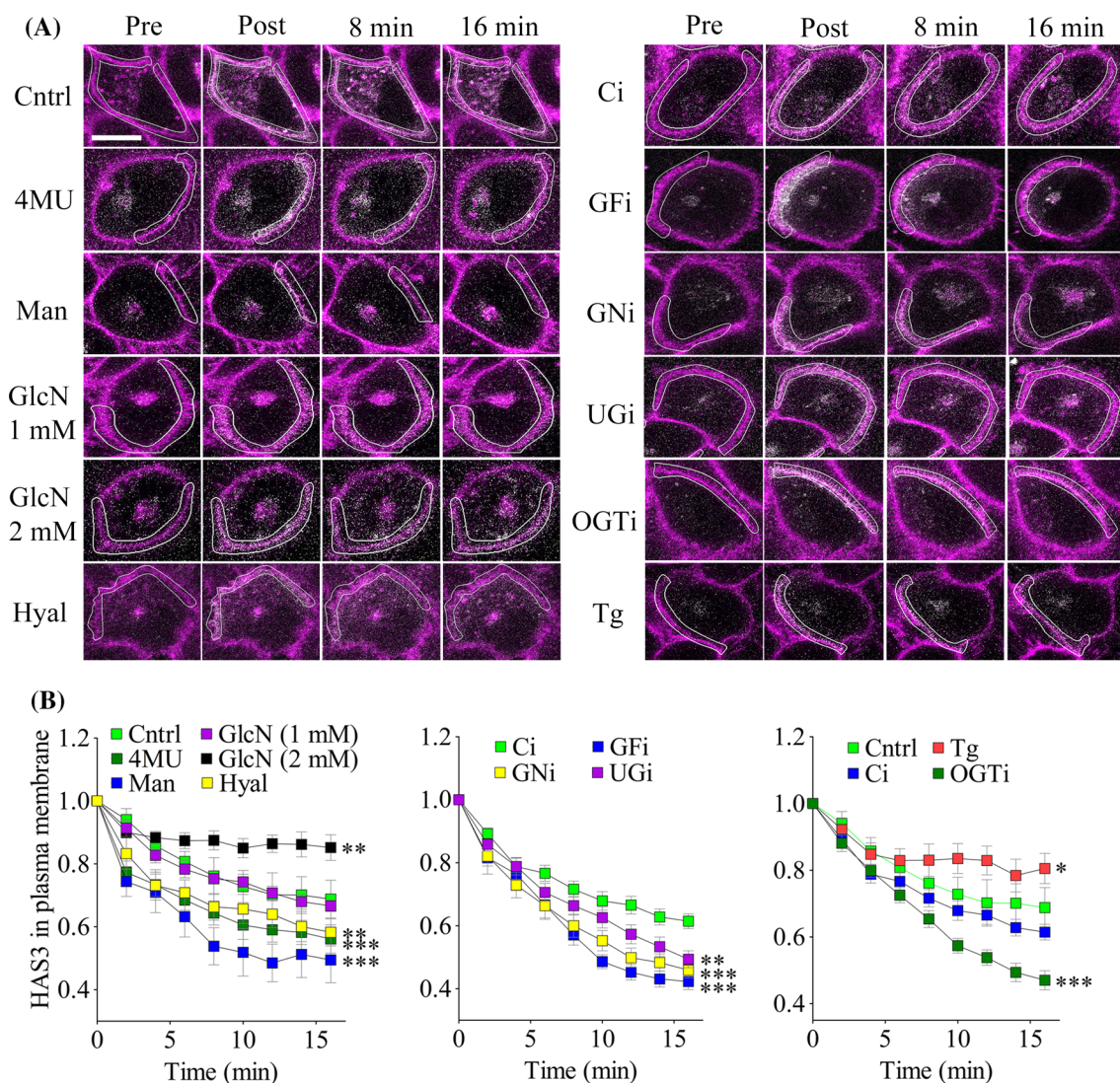


Fig. 3 Plasma membrane retention of HAS3 is regulated by UDP-sugar levels and O-GlcNAcylation. **a** Dendra2-HAS3 was photoconverted (pseudocolored as *white*) in plasma membrane, marked by *deep mask red* (*magenta*), and shown by the *white* region of interest. The disappearance from plasma membrane of the photoconverted Dendra2-HAS3 was monitored. Representative images are shown for the treatments. **b** Time lapse data of the photoconverted Dendra2-HAS3 remaining in plasma membrane was compiled to compare the

disappearance rates between the treatments. *Cntrl* control, *4MU* 4-methylumbelliferone, *Man* mannose, *GlcN* glucosamine, *Hyal* hyaluronidase, *Ci* control siRNA, *GF*i** GFAT siRNA, *GN*i** GNPDA1 and 2 siRNAs, *UG*i** UGDH siRNA, *OGT*i** OGT siRNA, *Tg* ThiametG. The data represent mean ± SEM values from five independent experiments, with ten images/group; **p* < 0.05, ***p* < 0.01, ****p* < 0.001 (one way ANOVA, Tukey's test). Scale bar 20 μm

reduced and enhanced, respectively, HAS3 disappearance from plasma membrane (Fig. 3b). The results thus suggest that both UDP-GlcNAc and UDP-GlcUA contents influence the level of HAS3 in plasma membrane by controlling its endocytosis, and O-GlcNAcylation accounts for at least a part of the effect of UDP-GlcNAc. The O-GlcNAcylation-dependent retention of HAS3 in plasma membrane is in line with the finding that O-GlcNAcylation enhances hyaluronan synthesis (Fig. 2i). During its processive synthesis, and even after it, hyaluronan chain remains tightly bound to HAS3. To probe the role of the hyaluronan chain

in the retention of HAS3 in plasma membrane, we stripped away cell surface hyaluronan with *Streptomyces* hyaluronidase. This resulted in a significantly enhanced endocytosis of Dendra2-HAS3 (Fig. 3b).

Since CD44 was abundant on the surface of these cells, we checked whether it was involved in HAS3 endocytosis. As shown in Suppl. Figure 3, siRNA suppression of CD44 expression did not affect endocytosis of Dendra2-HAS3. The above results suggest that hyaluronan chain under production, but not one attached with CD44, is a major determinant in the plasma membrane retention and kinetics of HAS3.

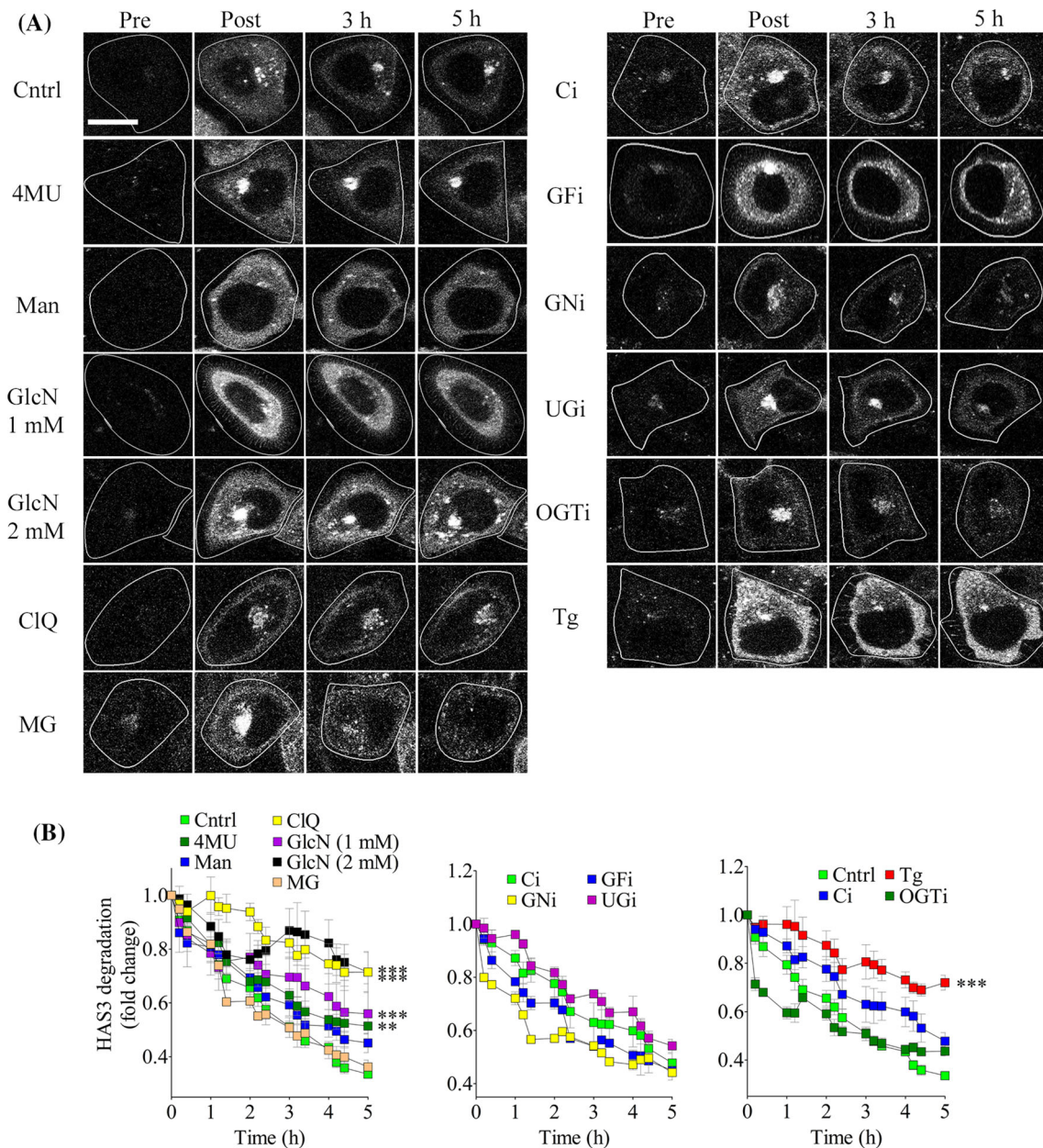


Fig. 4 UDP-GlcNAc surplus and O-GlcNAcylation prevent lysosomal degradation of HAS3. Dendra2-HAS3 was photoconverted (pseudocolored as white) in whole cells and its disappearance was monitored for 5 h. **a** Representative images from different treatments show the signal before photoconversion (Pre), immediately after (Post), and following 3–5 h chase. **b** The signal intensity of photoconverted Dendra2-HAS3, plotted as function of time, and

related to the post-conversion value. CIQ, chloroquine (0.1 mM), an inhibitor of lysosomal degradation; MG, MG132 (2.5 μM), an inhibitor of proteasomal degradation; other abbreviations as in Fig. 3. The data represent mean ± SEM from five independent experiments, with 5–7 images/group; ****p* < 0.001, ***p* < 0.01 (one way ANOVA, Tukey’s test). Scale bar 20 μm

Reduced HAS3 degradation by glucosamine and O-GlcNAcylation

The endocytosed Dendra2-HAS3 can be routed either to degradation or recycling. It was therefore important to check whether the UDP-sugars also influence overall degradation

rate of HAS3. This was studied in MV3 cells by Dendra2-HAS3 photoconversion in the entire cell, and examination of the disappearance rate of the red signal (Fig. 4a). The half-life of Dendra2-HAS3 in control cells was ~3 h (Fig. 4b). Blocking lysosomal function with chloroquine markedly slowed down the degradation, while the

proteasome inhibitor MG132 had no effect, indicating that Dendra2-HAS3 is degraded in lysosomes (Fig. 4). Cells treated with glucosamine showed a strong, dose-dependent reduction of Dendra2-HAS3 decay. Dendra2-HAS3 degradation was also blocked by enhanced O-GlcNAcylation by ThiametG. The decay rate was not affected by mannose, or siRNAs for the enzymes in the UDP-sugar biosynthesis pathways (GFAT1, GNPDA1 and 2, and UGDH), while 4MU slightly reduced Dendra2-HAS3 degradation (Fig. 4b). The data thus suggest that elevated O-GlcNAc signaling increases the overall half-life of HAS3.

UDP-sugar depletion and blocked O-GlcNAcylation increases HAS3 in early endosomes

A significant fraction of EGFP-HAS3 in MV3 cells was colocalized with early endosome antigen 1 (EEA1), a marker for early endosomes (Fig. 5a). This finding substantiates the rapid kinetics of Dendra2-HAS3 endocytosis from plasma membrane. Lowering the levels of UDP-GlcUA (4MU, UGDH siRNA) and UDP-GlcNAc (mannose, GFAT1 and GNPDA1 and 2 siRNA) further increased the colocalization of EGFP-HAS3 with EEA1, obviously reflecting the

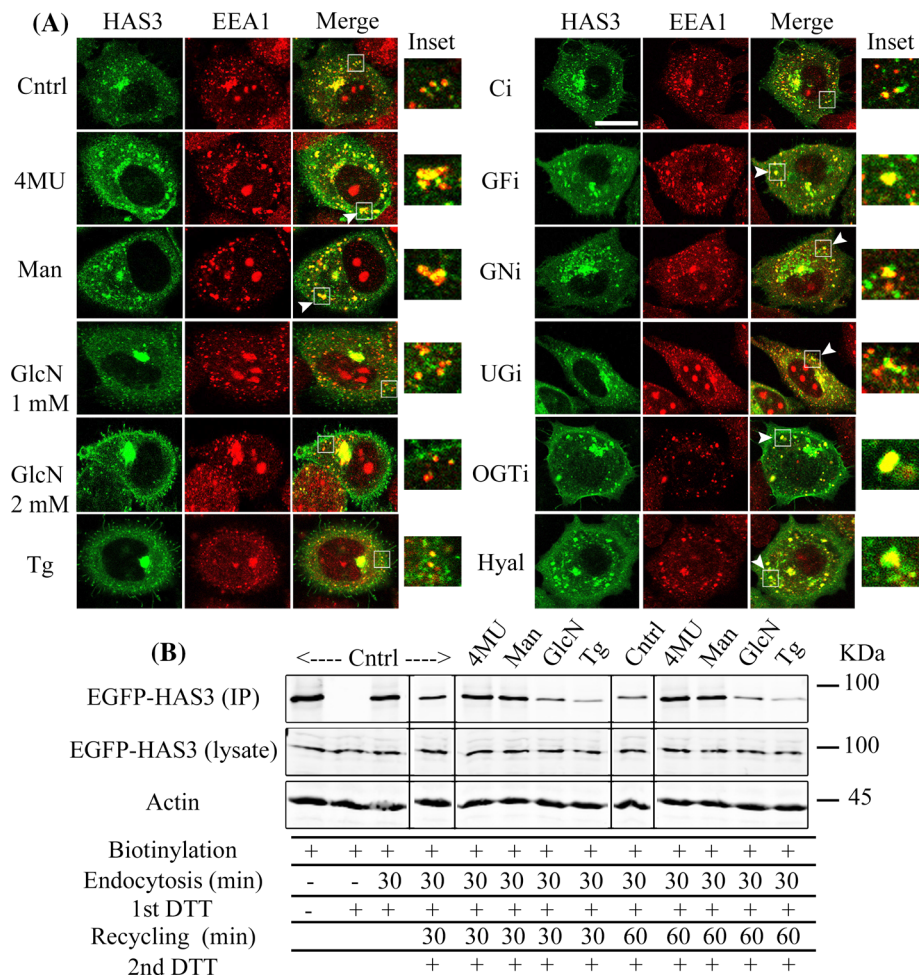


Fig. 5 UDP-sugar contents and O-GlcNAcylation affect HAS3 level in early endosomes and recycling to plasma membrane. **a** Representative images of MV3 cells, showing the doxycycline-induced EGFP-HAS3 (green) and EEA1 (an early endosome marker, red), and their colocalizations (yellow). In the “merge” column of images, a small region of interest with illustrative vesicular structures (white box) is shown enlarged in the adjacent inset. Arrowheads point to EGFP-HAS3 and EEA1 colocalized in vesicles, enlarged by treatments that deplete UDP-sugars, O-GlcNAcylation, or cell surface hyaluronan. Abbreviations are as in Figs. 3. and 4. Scale bar 20 μ m. **b** Cell surface proteins of COS1 cells transfected with EGFP-HAS3 were biotinylated. Biotinylated EGFP-HAS3 was detected by western blotting from cell lysates first immunoprecipitated (IP) with an EGFP

antibody and then with streptavidin-coated magnetic beads. Following biotinylation EGFP-HAS3 was allowed to be endocytosed for 30 min, and whatever remained on cell surface or was recycled back, was treated with DTT to remove biotin. Cells analyzed at this time therefore showed only intracellular biotinylated EGFP-HAS3. After this clearing of the cell surface biotinylated EGFP-HAS3, the incubation was continued for 30 or 60 min to allow the intracellular EGFP to return to plasma membrane, then stripped by DTT again, and analyzed for the intracellular signal. To facilitate visual comparison of the recycling rates, copies of the control lanes were pasted on the left side of the 30 and 60 min second DTT stripping of the treated cells (all bands originate from a single gel). The same result was obtained in two independent experiments

enhanced endocytosis noted with Dendra2-HAS3. In contrast, by increasing the levels of UDP-GlcNAc with glucosamine, the colocalization of EGFP-HAS3 with EEA1 was decreased (Fig. 5a). Moreover, the EGFP-HAS3-positive vesicular structures were enlarged in cells with depleted UDP-sugars, while those in glucosamine-treated cells were small, and reduced in numbers, as compared to controls (Fig. 5a). Reduced numbers and sizes of the EGFP-HAS3-positive early endosomes were also found when O-GlcNAcylation was increased by ThiametG, while larger EGFP-HAS3- and EEA1-positive endosomes were noted in cells treated with OGT siRNA. Hyaluronidase, another stimulator of HAS3 endocytosis, also increased EGFP-HAS3 colocalization with EEA1 in large endosomes (Fig. 5a), and accumulation of photoconverted Dendra2-HAS3 near plasma membrane (Suppl. Figure 4). The abundance of HAS3 in early endosomes thus closely correlates with the rate of HAS3 endocytosis and the EEA-positive vesicles thus receive HAS3 not retained in plasma membrane.

Regulation of HAS3 recycling by UDP-sugars

The short half-life of HAS3 in plasma membrane (min), as compared to total degradation (h) suggested that after endocytosis not all of the HAS3 in early endosomes is routed to lysosomes, but could be recycled back to plasma membrane. To demonstrate this, we used COS1 cells, since this cell line, unlike MV3, tolerates the rapid changes in temperature needed in this assay. We labeled the extracellular domains of EGFP-HAS3 with a dithiothreitol (DTT)-cleavable biotin, and detected the label in immunoprecipitated EGFP-HAS3. Immediately after labeling, all biotin on EGFP-HAS3 was susceptible to

cleavage by extracellular DTT (Fig. 5b). During a 30 min chase, a large part of the labeled EGFP-HAS3 was endocytosed, and became resistant to DTT (see the left lanes marked with “Cntrl” in Fig. 5b). Following another 30–60 min chase, and a second DTT treatment, more EGFP-HAS3 had disappeared, indicating that it had returned to plasma membrane and be cleaved. When cultures subjected to the above protocols were treated with 4MU or mannose, a larger part remained uncleaved, indicating that less of it had returned to plasma membrane. In contrast, cultures treated with glucosamine or ThiametG showed less biotinylated EGFP-HAS3 after the treatments, indicating that more of the biotinylated EGFP-HAS3 had returned to plasma membrane, and got cleaved with DTT.

As shown above, there is a continuous flux of HAS3-positive vesicles fusing into plasma membrane, and a simultaneous flux of HAS3 that end up in early endosomes. TIRF microscopy was applied to study the appearance and disappearance of these EGFP-HAS3-positive vesicles in MV3 cells in the cytoplasmic zone 100–200 nm under plasma membrane. Images of the TIRF zone vesicles, changing with time and location, are shown in Fig. 6. The activity of this vesicular traffic was quantitated with 70 s recordings of the vesicle numbers in the TIRF zone. The amplitude of the changes in the vesicle numbers was considered to reflect the recycling activity (Fig. 7a–d). Depletion of the UDP-sugars by 4-MU, mannose, and the siRNAs targeting their synthesis, reduced the rate of recycling, as indicated by the HAS3 traffic under plasma membrane (Fig. 7e). In contrast, a glucosamine-induced surplus of UDP-GlcNAc increased the sub-membrane HAS3 traffic. Increasing cellular O-GlcNAcylation by ThiametG and its reduction by OGT siRNA, enhanced and

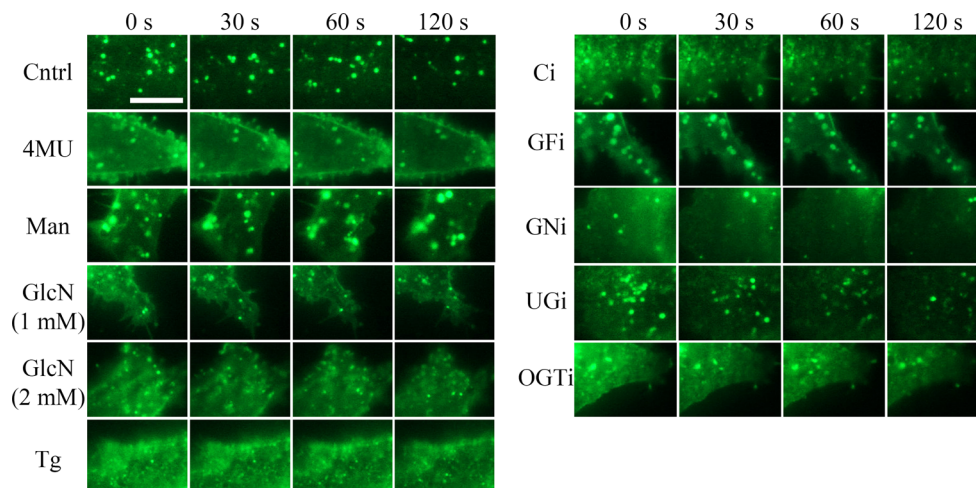
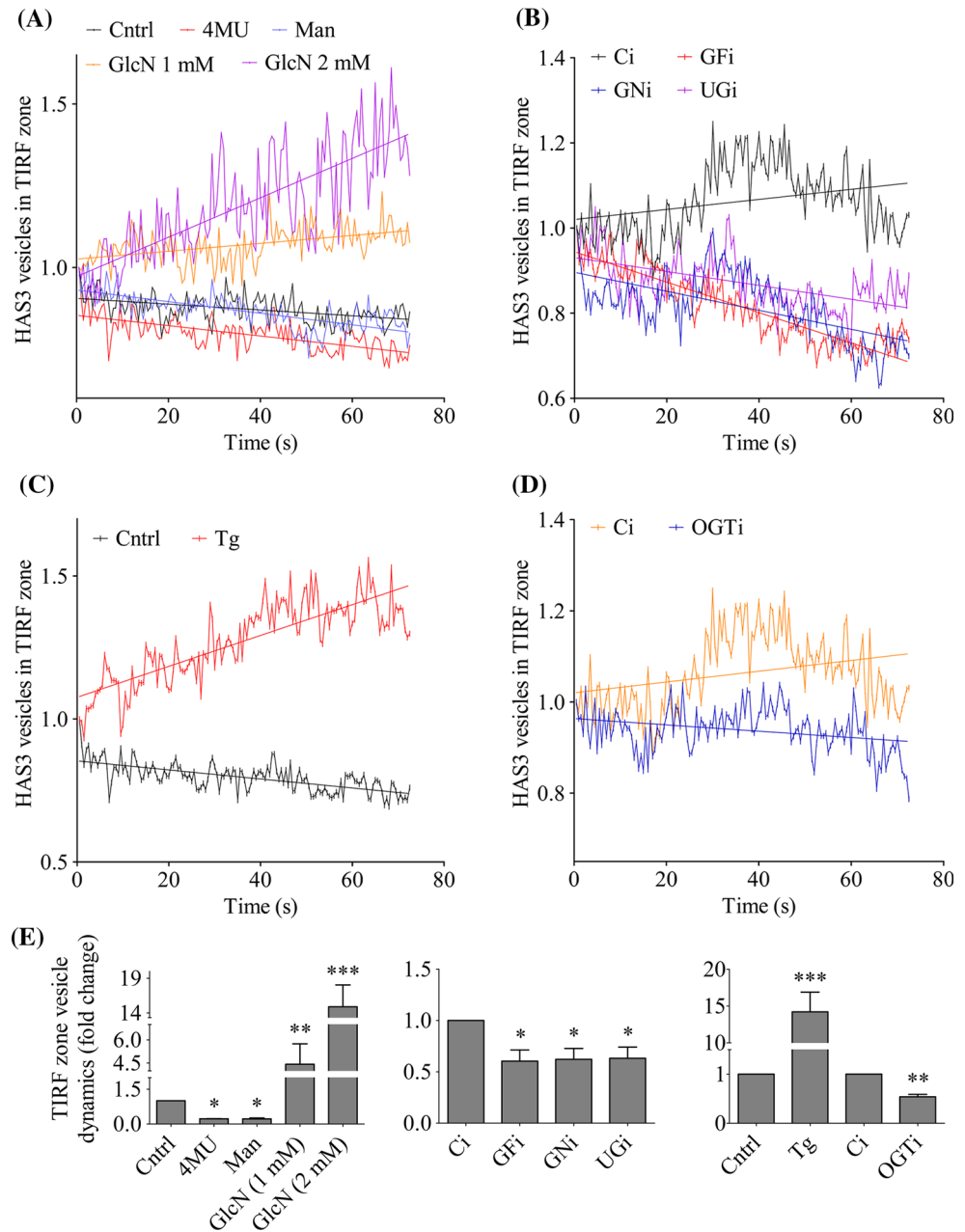


Fig. 6 UDP-sugar levels and O-GlcNAcylation regulate vesicular traffic of HAS3 at plasma membrane. Illustration of the changes in the numbers and locations of the EGFP-HAS3-positive vesicles in the TIRF zone under the plasma membrane of MV3 cells. An enlarged part of the cell is shown here for the clarity of vesicles in each of the

time points between 0–120 s. Scale bar 10 μ m. The data shows representative images from 3–5 independent experiments, with 7–10 images/group. There were on the average 60–80 vesicles per image at the beginning of the recording, and the treatment groups did not differ from each other in this respect. Abbreviations are as in Figs. 3 and 4

Fig. 7 Dynamics of HAS3 vesicles under plasma membrane in MV3 cells. **a–d** The number of EGFP-HAS3 vesicles in the TIRF zone (see Fig. 6) was counted at 0.5 s intervals for 72 s. A linear regression (trend) line was calculated for the data points, indicated in the graphs. Based on the equation obtained from the regression line, standard deviation (SD) was calculated for each data point (see “Materials and methods” for detailed explanation). **e** The mean values of the SDs were considered to represent the rate of HAS3 traffic under plasma membrane (TIRF zone). The means of the SDs thus obtained were normalized to control or control siRNA and shown as fold change. *Cntrl* control, *4MU* 4-methylumbelliferone, *Man* mannose, *GlcN* glucosamine, *Ci* control siRNA, *GFi* GFAT siRNA, *GNi* GNPDA1 and 2 siRNAs, *UGi* UGDH siRNA, *OGTi* OGT siRNA, *Tg* ThiametG. The data represent mean values (a–d) or mean \pm SEM (e) from 3–5 independent experiments, with 7–10 images/group. *** $p < 0.001$, ** $p < 0.01$, * $p < 0.05$ (one way ANOVA, Tukey’s test)



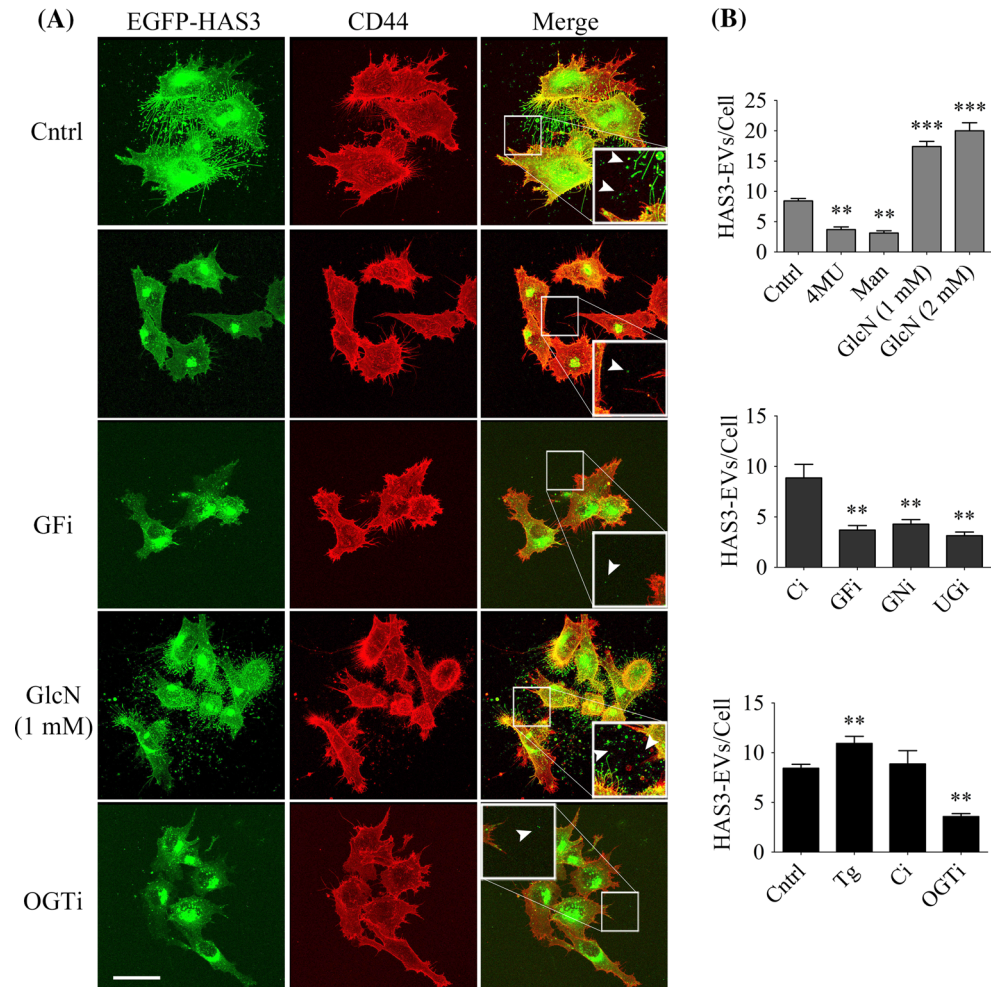
blocked, respectively, the vesicular traffic of HAS3 under plasma membrane (Fig. 7e). The findings suggest that a high level of the UDP-sugar substrates and/or O-GlcNAcylation push HAS3 vesicles towards plasma membrane, while UDP-sugar depletion suppresses this traffic to plasma membrane.

UDP-sugars control HAS3 shedding into extracellular vesicles

We have noted previously considerable amounts of HAS3 in HA-coated extracellular vesicles (EVs) [34]. EVs are recently

recognized vehicles for intercellular communication suggested to favor cancer development, for example. MV3 melanoma cells, induced to overexpress EGFP-HAS3, were cultured in a 3D collagen matrix that allows retention and imaging of the EVs in cell vicinity (Fig. 8a). Quantitation of the EVs showed that decreasing UDP-GlcUA (Fig. 8b: 4MU and UGi) or UDP-GlcNAc (Fig. 8b: Man, GFi and GNi) significantly reduced the shedding of EGFP-HAS3-positive EVs, while increased UDP-GlcNAc levels (Fig. 8b: GlcN) enhanced their shedding. These data thus indicate that the flux of HAS3 into EVs is directly correlated with the level of the cytosolic UDP-sugars, the presence of HAS3 in plasma

Fig. 8 Shedding of HAS3-positive extracellular vesicles is controlled by UDP-sugar levels and O-GlcNAcylation. **a** MV3-EGFP-HAS3 cells, grown in a type I collagen-based 3D matrix were induced for 24 h with 0.25 $\mu\text{g}/\text{ml}$ doxycycline to express EGFP-HAS3. Representative images of cultures with different numbers of the extracellular vesicles (*arrowheads*) in the adjacent matrix are shown, with the hyaluronan receptor CD44 (*red*) as a marker for plasma membrane. *Scale bar* 20 μm . **b** Extracellular vesicle counts per cell, calculated from compressed stacks of confocal images. Abbreviations as in Figs. 3, 4, 5 and 6. The data represent mean \pm SEM from three independent experiments, with 10–15 images/group; *** $p < 0.001$, ** $p < 0.01$ (one way ANOVA, Tukey's test)



membrane, and hyaluronan synthesis. Shedding of HAS3-positive EVs was also significantly increased with elevated O-GlcNAcylation (Fig. 8b: Tg), and decreased with reduced O-GlcNAcylation (Fig. 8b: OGTi). Since HAS3 overexpression and hyaluronan synthesis result in mitotic spindle misorientation, disturbed epithelial cell polarity [35], enhanced shedding of EVs [34], and cancer progression [24], we wanted to know whether the UDP-sugars, could also be involved in cellular functions related to carcinogenesis.

UDP-sugars affect basic cellular functions

We checked whether UDP-GlcUA and UDP-GlcNAc levels, and the consequent changes in hyaluronan synthesis and O-GlcNAc signaling, affect some basic functions in HAS3 expressing MV3 cells. With suppressed UDP-GlcNAc synthesis (GFATi and GNPDA1 and 2i) the proliferation of MV3-HAS3 cells was slightly increased, while 4MU, mannose and 1 mM glucosamine inhibited proliferation (Fig. 9a). Increased O-GlcNAcylation with ThiametG showed a tendency to enhance cell proliferation, though

statistical significance for an effect was not reached (Fig. 9a: Tg). However, decreased O-GlcNAcylation with OGTi (Fig. 9a: OGi), and decreased UDP-GlcUA synthesis with UGDHi (Fig. 9a: UGi) had no influence. Adhesion of MV3-HAS3 cells to type I collagen was enhanced in cells with decreased levels of UDP-GlcNAc or UDP-GlcUA, and faster adhesion was also noted with suppressed O-GlcNAcylation (OGT siRNA) (Fig. 9b: OGTi). Unexpectedly, faster adhesion was also found in cells with glucosamine-induced increase of UDP-GlcNAc (Fig. 9b: GlcN). In a scratch-wound assay 4MU and 1 mM glucosamine strongly inhibited, while mannose stimulated migration (Fig. 9c).

In summary, while interference with UDP-sugar metabolism showed strong effects on many cellular functions, these effects were apparently not associated just with hyaluronan synthesis, but probably reflected also multiple, divergent targets in cellular O-GlcNAc signaling and energy metabolism, the sum effect of which was unpredictable considering the many factors that eventually determine proliferation, adhesion and migration.

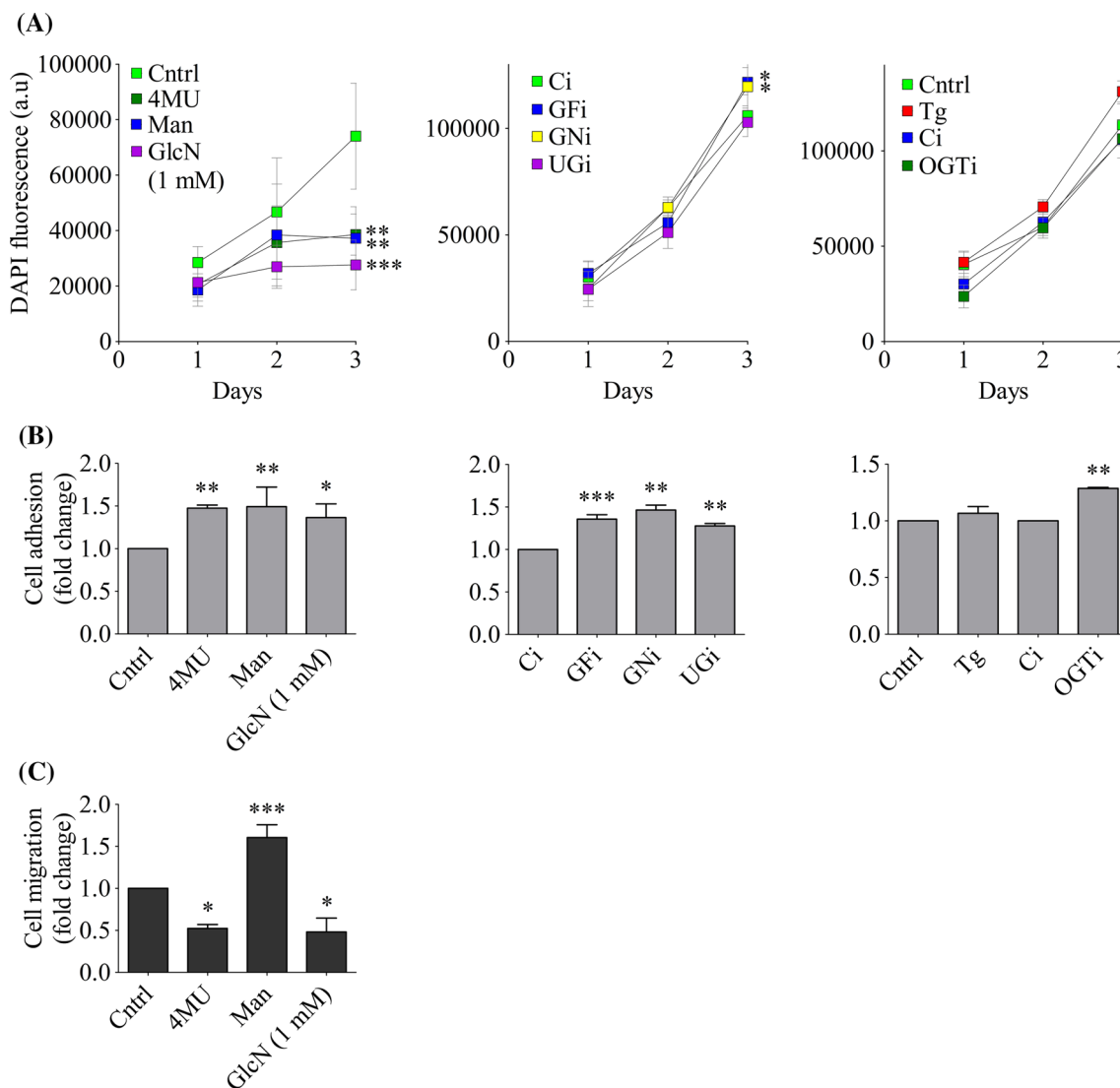


Fig. 9 Effect of UDP-sugar levels and O-GlcNAcylation of HAS3 on basic cellular functions. **a** MV3-EGFP-HAS3 cells in 96-well plates were induced with 0.05 $\mu\text{g}/\text{ml}$ doxycycline for 24 h, treated with chemicals and siRNAs (as explained in “Materials and methods”), and the cells were grown in the presence of chemicals in fresh media or just in fresh media in case of siRNA treatment. The cell proliferation was estimated 1–3 days later by fluorescence of DAPI incorporated in the nuclei. **b** MV3-EGFP-HAS3 cells were induced with 0.1 $\mu\text{g}/\text{ml}$ doxycycline for 24 h, treated with chemicals and siRNAs as mentioned above, trypsinized and allowed to adhere for 30 min to 96-well plates coated with type I collagen. After washing,

the number of cells attached was analyzed by MTT reactions as described in “Materials and methods”. **c** MV3-EGFP-HAS3 cells were induced with 0.05 $\mu\text{g}/\text{ml}$ doxycycline for 24 h, treated with chemicals as mentioned above, and the cells were grown in the presence of chemicals in fresh media. A scratch wound assay was performed to measure cell migration. *Cntrl* control, *4MU* 4-methylumbelliferone, *Man* mannose, *GlcN* glucosamine, *Ci* control siRNA, *GF*i** GFAT siRNA, *GN*i** GNPDA1 and 2 siRNAs, *UG*i** UGDH siRNA, *OGT*i** OGT siRNA, *Tg* ThiametG. The data represent mean \pm SEM from 3–5 independent experiments; * $p < 0.05$, ** $p < 0.01$, *** $p < 0.001$ (one way ANOVA, Tukey’s test)

Enzymes related to UDP-sugar metabolism in human melanoma

As changes in UDP-sugar content influenced the above mentioned cellular functions and since hyaluronan is considered a major player in different malignancies, we wanted to know how UDP-sugar metabolism changes in cancer. While little data are available on UDP-sugar content in any cancer, information on the expression of enzymes involved

in UDP-sugar biosynthesis is available (OncomineTM Research Edition; <http://www.oncomine.org>). For example, mRNA levels of GFAT1 and UGDH are elevated in breast cancer, while GNPDA1 and UGDH are decreased in kidney cancer. Unfortunately there are no studies on the protein levels of these enzymes in tumors, or data on possible correlation between hyaluronan content and UDP-sugars. For a pilot exploration of these issues we chose melanoma, a tumor showing stage-dependent changes in hyaluronan

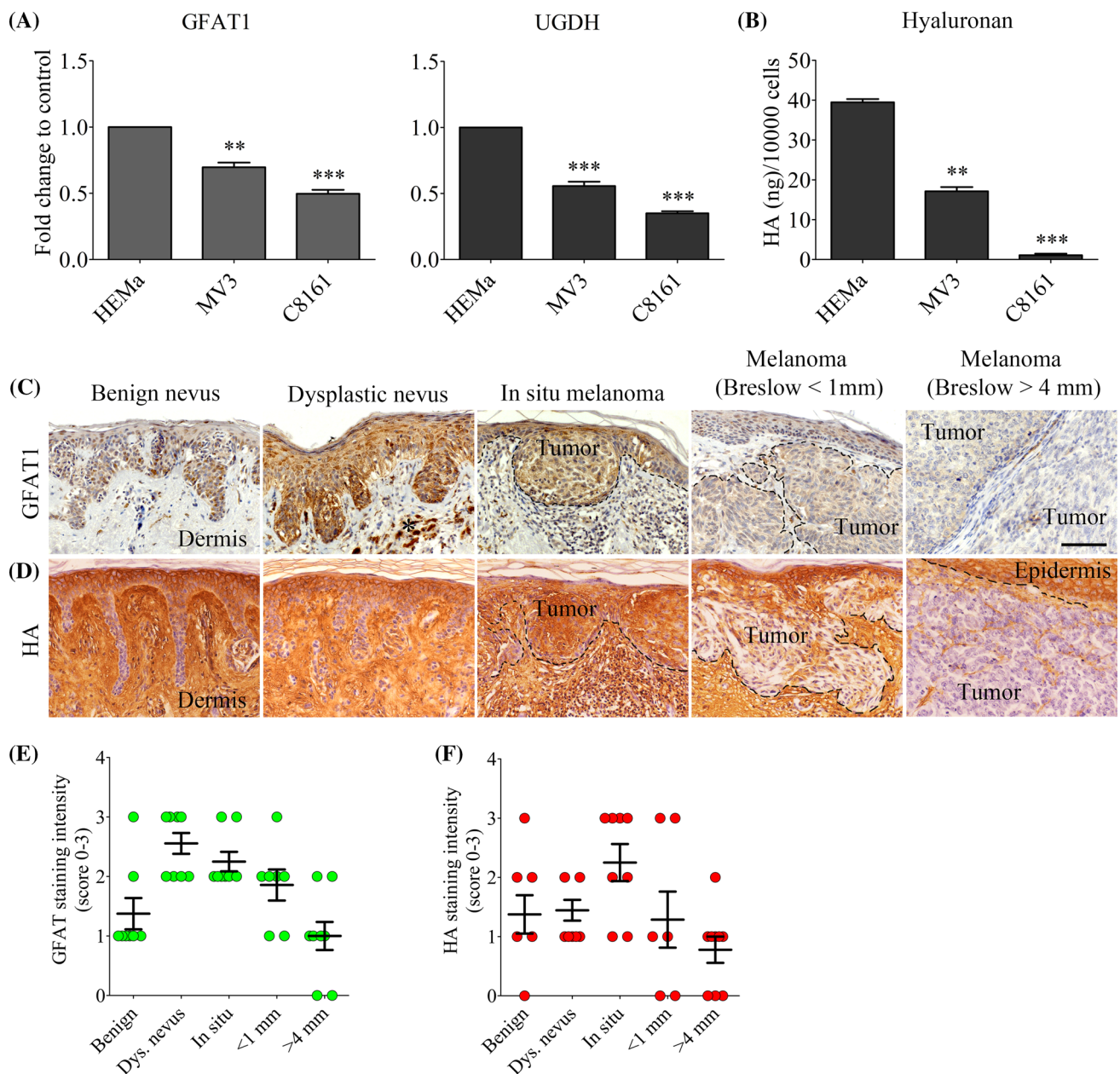


Fig. 10 Expression of GFAT1, UGDH and hyaluronan in human melanocytic cells and tissue biopsies. **a** GFAT1 and UGDH mRNA levels were quantitated by real-time Q-PCR in a primary melanocytic cell line (HEMa) and two melanoma cell lines (MV3 and C8161) with different metastatic capacity (mean \pm SEM from three independent experiments). **b** Hyaluronan content per cell in the growth medium of the cell lines after 24 h incubation (mean \pm SEM from three independent experiments). Examples of **c** GFAT1 and **d** hyaluronan (HA) reactivity (brown) with hematoxylin (blue) counterstaining for

nuclei, in human skin tissue sections expected to represent different stages of melanoma progression. Tumor area is marked with *dash lines* in in situ melanoma and in < 1 mm melanoma. *Asterisk* points to melanin in dysplastic nevus. **e, f** Scoring of GFAT1 and hyaluronan staining intensities in the same stages as above. Individual patient samples are indicated as *circles*, means and SEM as *horizontal and vertical bars*. The data represent mean \pm SEM from 7–9 patients/group. *** p < 0.001, ** p < 0.01 (one way ANOVA, Tukey's test). Scale bar 50 μ m

content, i.e. compared to benign nevus, hyaluronan content first increases in in situ melanoma, and then decreases in invasive melanomas [22, 39]. Since tissue samples were not available for biochemical analysis of UDP-sugars, we used cultured cell lines and paraffin blocks originally used for diagnostic purposes, representing different stages of

melanomas. The relative mRNA levels of the two rate limiting enzymes in UDP-sugar biosynthesis, i.e. GFAT1 and UGDH, declined from the normal primary melanocyte (HEMa) through MV3 to C8161, reflecting increasing aggressiveness (Fig. 10a) and correlating with declining hyaluronan synthesis (Fig. 10b). The immunohistochemical

staining intensity of GFAT1 was significantly increased in dysplastic nevi and in situ melanoma, when compared to benign nevi, while its expression gradually declined in invasive melanomas (<1 and >4 mm invasion) (Fig. 10c, e). This GFAT1 staining pattern in different melanoma stages corresponded to that of hyaluronan (Fig. 10d, f) [39], suggesting that UDP-sugar metabolism closely follows the synthesis of hyaluronan, and perhaps initiates and supports the progression of melanoma in its different stages.

Discussion

The synthesis of hyaluronan, as other bulky cell surface polysaccharides like chitin and cellulose, takes place in plasma membrane in order to deliver the product directly into extracellular space [47]. This implies that the enzymes responsible must be transported from Golgi to plasma membrane for activation. The transport of the enzymes is therefore an integral part of the polysaccharide synthesis, but has received little attention. The present study shows for the first time that the vesicular traffic of the HAS3 enzyme is subject to strict regulation by the cytoplasmic availability of UDP-GlcNAc and UDP-GlcUA, the precursors of hyaluronan, and substrates of the HAS3 enzyme.

Roles of UDP-sugars on hyaluronan synthesis and other cell functions

The influence of the UDP-sugars on HAS3 transport, and hyaluronan synthesis as a consequence, means that hyaluronan synthesis is subject to regulation by the metabolic state of the cell, since glucose has a strong impact on the concentration of UDP-sugars [33]. However, the cytoplasmic level of UDP-GlcNAc is not only important for hyaluronan synthesis, but acts as a general indicator of glucose supply, and metabolic status of the cell [5]. It controls a number of vital functions through O-GlcNAcylation of cytoplasmic, nuclear [11], and even mitochondrial proteins [2, 11]. The important role of the UDP-sugars in the cellular phenotype was demonstrated here by the diversity of their effects in proliferation, adhesion and migration, many of which are known to be dependent on hyaluronan [1, 8, 26, 45]. Therefore, two cellular functions, hyaluronan synthesis and the O-GlcNAc signaling, are particularly sensitive to changes in the cellular content of UDP-GlcNAc. It is actually surprising how little is known about UDP-GlcNAc associations with various phenotypic features of cells.

Comparison of UDP-GlcUA and UDP-GlcNAc effects on HAS3 traffic

The present study shows that the trafficking of HAS3 depended on both UDP-GlcNAc and UDP-GlcUA,

probably present in limiting concentrations for full activity of HAS3. Previous studies have suggested that their cellular concentrations roughly match the K_m values of HAS3 for these substrates [16]. However, while UDP-GlcUA affected the plasma membrane presence of HAS3, i.e. its endocytosis and recycling, unlike UDP-GlcNAc it did not influence the lysosomal decay of HAS3 (Fig. 11). It is therefore concluded that UDP-GlcNAc had additional functions in HAS3 trafficking besides a substrate of HAS3. These functions were obviously mediated by stimulation of O-GlcNAcylation, since increasing O-GlcNAcylation with ThiametG reproduced the effect of high UDP-GlcNAc supply (see Fig. 2d, m).

Traffic of HAS3 from Golgi to plasma membrane

The effects of UDP-sugars on the forward traffic from Golgi to plasma membrane were difficult to interpret. The relative content of HAS3 was very high in the Golgi, suggesting that it served as a maturation and/or storage site for the enzyme. Perhaps therefore the proportional disappearance rate of HAS3 from Golgi area was slow, as compared for instance to the traffic at cell surface. The residence time of HAS3 in the Golgi area is probably controlled by several different and contradictory processes as suggested by the findings that the depletion of HAS3 from Golgi area was enhanced by most treatments—whether UDP-sugars and O-GlcNAcylation were increased or decreased. It became also clear that assays of the slow arrival of Golgi-labeled HAS3 in cell surface, which was reduced by almost all treatments, was muddled by the rapid kinetics of HAS3 vesicular traffic at plasma membrane. These data actually favor the idea that HAS3 did not travel directly from Golgi to plasma membrane, but that there was an intermediate, probably endosomal compartment in the traffic of HAS3 between Golgi and plasma membrane. A similar indirect route to plasma membrane has been shown for other cargos like interleukin 6 (IL6) and tumor necrosis factor α (TNF α) [25, 27].

Endocytosis and plasma membrane recycling of HAS3

The present findings indicated that a large proportion of HAS3 arriving at plasma membrane is rapidly endocytosed back into cytoplasm and localized in early endosomes. An important result was that UDP-GlcNAc surplus stimulated the rate of HAS3 vesicular traffic adjacent to plasma membrane, with a net effect of reduced endocytosis rate. In contrast, depletion of UDP-GlcNAc and UDP-GlcUA reduced the cortical traffic of vesicles containing HAS3, resulting in decreased plasma membrane half-life of HAS3 and its accumulation in the enlarged early endosomes

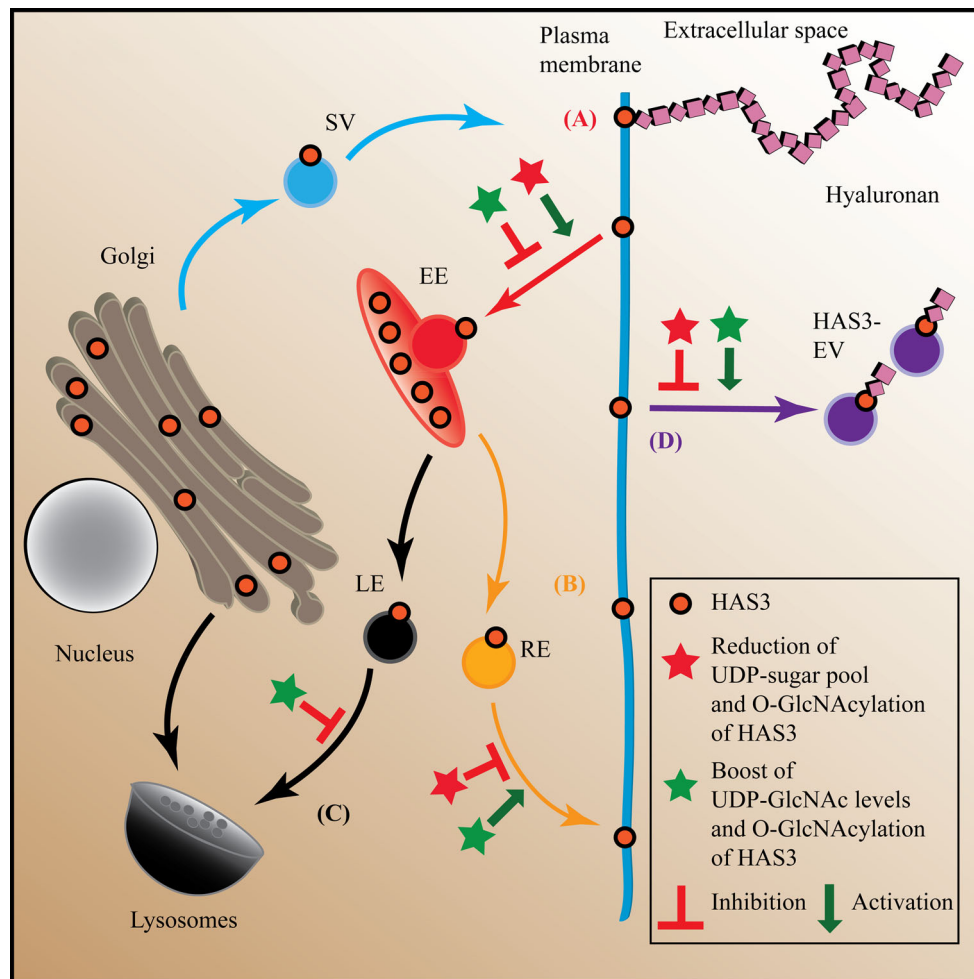


Fig. 11 Illustration of HAS3 traffic regulated by UDP-sugar levels and O-GlcNAcylation of HAS3. **a** HAS3 present in plasma membrane synthesizes hyaluronan (pink chain) into extracellular space. When there is a shortage of UDP-sugars as substrates, or hyaluronan is degraded, endocytosis of HAS3 is enhanced. On the other hand, surplus of UDP-sugar supply increases the residence of HAS3 in plasma membrane. Increased and decreased O-GlcNAcylation of HAS3 due to excess UDP-GlcNAc supply also respectively inhibits and accelerates the endocytosis of HAS3 from plasma membrane. With increased endocytosis of HAS3 due to shortage of supply of UDP-sugars and reduced O-GlcNAcylation, HAS3 is accumulated in early endosomes. **b** The internalized HAS3 is actively recycled back

to plasma membrane when there is an increased supply of UDP-sugars and enhanced O-GlcNAcylation of HAS3. In contrast, there is relatively less recycling of HAS3 if the level of UDP-sugars and O-GlcNAcylation of HAS3 is reduced. **c** Abundant cellular levels of UDP-GlcNAc and increased O-GlcNAcylation increase the half-life of HAS3 by inhibiting its lysosomal degradation. **d** Shedding of HAS3-containing extracellular vesicles is triggered by abundant UDP-sugar levels and increased O-GlcNAcylation of HAS3. On the other hand, reduced UDP-sugar levels and O-GlcNAcylation of HAS3 curtails that. *SV* secretory vesicles, *EE* early endosomes, *RE* recycling endosomes, *LE* late endosomes, *HAS3-EV* HAS3-derived extracellular vesicles

(Fig. 11). Details of the HAS3 uptake need to be further explored, but we have previously shown that Rab10 is a component of the HAS3 endocytosis machinery [8].

Another important result was that once endocytosed, HAS3 could be recycled back to plasma membrane. This was shown by the return to plasma membrane of endocytosed HAS3 that was originally biotinylated on cell surface. The strong influence of UDP-sugars was also demonstrated in the recycling experiment. A larger proportion of recycled HAS3 was on the surface of cells with a surplus of UDP-GlcNAc, while less of the recycled HAS3 was present in plasma membrane following depletion of either

UDP-GlcUA or UDP-GlcNAc. It can be concluded that recycling increases the constant feed of new HAS3 to plasma membrane.

Recycling of HAS3 and stochastic initiation of hyaluronan chains

The rapid traffic of HAS3 at plasma membrane appears incompatible with the data available on the time required for the production of an intact hyaluronan chain, which has a molecular mass above 2×10^6 Da, with >10,000 monosaccharide units [4, 36]. However, it is likely that the

average half-life measured here mainly reflects the majority of HAS3 that rapidly recycles at plasma membrane, and tends to overwhelm those HAS3 molecules involved in hyaluronan synthesis.

HAS3 is a processive enzyme tightly attached to the growing polymer [15, 57]. A hyaluronan chain protruding into the extracellular space may initially reduce the likelihood of HAS3 endocytosis, and later chain growth completely prevents it. The idea that attached hyaluronan retains HAS3 in plasma membrane was supported by the fact that cleavage of the hyaluronan by hyaluronidase increased the average rate of HAS3 endocytosis, and increased HAS3 localization in early endosomes. The effects of the UDP-sugars on HAS3 endocytosis can thus be understood by assuming that the concentration of these substrates determines the probability of hyaluronan chain initiation during the normally short visit of HAS3 in plasma membrane.

While hyaluronan chain keeps HAS3 in plasma membrane, the present findings suggest that the chain does not need to be anchored to CD44 for the retention of the HAS3-hyaluronan complex in plasma membrane, since HAS3 endocytosis was not affected by CD44 knockdown.

Termination of hyaluronan chain synthesis and HAS3 shedding in extracellular vesicles

The mechanism of hyaluronan chain termination is not known. Our present and previous work has shown that sometimes hyaluronan synthesis is not actually terminated at all in the sense that it would be detached from HAS3. Instead, both HAS3 and the attached hyaluronan are shed together on extracellular vesicles [34]. The present study indicated that UDP-sugar contents and O-GlcNAcylation also controlled the shedding of these HAS3-positive and hyaluronan-coated vesicles (Fig. 11), the shedding rate being directly correlated with the abundance of HAS3 in plasma membrane, and hyaluronan synthesis. The proportion of HAS3 endocytosed versus that is shed in extracellular vesicles is difficult to quantitate. However, the overall HAS3 disappearance rate in cells was slower with high UDP-GlcNAc content and O-GlcNAcylation, speaking against a significant extracellular loss in these conditions that enhanced vesicular shedding. Since the release of extracellular vesicles and their cargos are often associated with tumor progression and metastasis in several cancers [3, 32, 59], regulation of HAS3 shedding in extracellular vesicles by cytosolic UDP-sugar levels can be speculated to have an impact on cancer progression.

O-GlcNAcylation

O-GlcNAcylation or O-GlcNAc signaling was tightly involved in all aspects of the transport of HAS3, including its rate of subcortical trafficking, shedding in extracellular

vesicles, endocytosis, and lysosomal degradation. In all these aspects, increased O-GlcNAcylation reproduced the effects of UDP-GlcNAc surplus (Fig. 11). Indeed, it is difficult to make a distinction between the roles of UDP-GlcNAc as a substrate of HAS3, and as a stimulator of O-GlcNAc signaling, but the current experiments favor the importance of O-GlcNAcylation. O-GlcNAcylation was recently found also in HAS2, another member of the hyaluronan synthase family [54]. The modification was associated with increased overall half-life of the enzyme, and we are currently exploring the trafficking of HAS2 in more detail. It has been found that O-GlcNAcylation of cargo proteins influences their recruitment to transport vesicles [7, 10, 60]. This could be the case also with HAS3.

UDP-sugars and hyaluronan in cancer

While the synthesis and metabolism of hyaluronan are known to have a major impact on different aspects of many malignancies [13, 17, 38, 42, 43, 58], there is still little understanding on the molecular machineries leading to the changes in tumor hyaluronan synthesis. We raised the hypothesis that UDP-sugar metabolism is associated with the changes in tumor hyaluronan content and took skin melanoma as an example to test the hypothesis, since hyaluronan level correlates with the stage (grade) of the tumor: elevated levels are found in the early phase (in situ melanoma), followed by a clear reduction of hyaluronan in the more invasive stages of the malignancy [22, 39]. The hypothesis was supported in the present study by the immunohistochemical analysis of GFAT1, the rate-limiting enzyme in the biosynthesis of UDP-GlcNAc, as its staining intensity correlated with that of hyaluronan. The levels of GFAT1 and UGDH mRNA from cell lines representing different stages in melanoma development were also correlated with hyaluronan synthesis.

In summary, the present study describes novel regulatory mechanisms governed by UDP-sugars in hyaluronan synthesis, i.e. the intracellular trafficking and extracellular shedding of HAS3. The control mechanisms reveal the significance of these glucose metabolites in hyaluronan synthesis, which is particularly important in the interactions of malignant cells with their microenvironment, and hence the progression of tumors, like melanoma.

Acknowledgments We thank Dr. Raquel Melero for her expert guidance in image analysis, Avinash Bathina and Eija Rahunen for technical assistance and Veli-Pekka Ronkainen (Biocenter Oulu) for help in TIRF microscopy. This work was supported by the Sigrid Juselius Foundation (M.T. and R.T.), Kuopio University Hospital VTR funds (M.T.) and Spearhead Funds from University of Eastern Finland (Cancer Center of Eastern Finland) (M.T. and R.T.). Personal grants to A.J.D. from Finnish Cultural Foundation, Northern Savo Cancer Foundation, K. Albin Johanssons Stiftelse Foundation,

Doctoral Program in Molecular Medicine (DPMM), University of Eastern Finland, Finnish Glycoscience Graduate School and CIMO Foundation are gratefully acknowledged.

Compliance with ethical standards

Conflict of interest The authors declare there is no conflict of interest.

References

- Bakkers J, Kramer C, Pothof J, Quaadvlieg NE, Spaik HP, Hammerschmidt M (2004) Has2 is required upstream of Rac1 to govern dorsal migration of lateral cells during zebrafish gastrulation. *Development* 131:525–537
- Banerjee PS, Ma J, Hart GW (2015) Diabetes-associated dysregulation of O-GlcNAcylation in rat cardiac mitochondria. *Proc Natl Acad Sci USA* 112:6050–6055
- Beckham CJ, Olsen J, Yin PN, Wu CH, Ting HJ, Hagen FK, Scosyrev E, Messing EM, Lee YF (2014) Bladder cancer exosomes contain EDIL-3/Del1 and facilitate cancer progression. *J Urol* 192:583–592
- Bodevin-Authelet S, Kusche-Gullberg M, Pummill PE, DeAngelis PL, Lindahl U (2005) Biosynthesis of hyaluronan: direction of chain elongation. *J Biol Chem* 280:8813–8818
- Buse MG (2006) Hexosamines, insulin resistance, and the complications of diabetes: current status. *Am J Physiol Endocrinol Metab* 290:E1–E8
- Cayli A, Hirschmann F, Wirth M, Hauser H, Wagner R (1999) Cell lines with reduced UDP-*N*-acetylhexosamine pool in the presence of ammonium. *Biotechnol Bioeng* 65:192–200
- Cole RN, Hart GW (1999) Glycosylation sites flank phosphorylation sites on synapsin I: O-linked *N*-acetylglucosamine residues are localized within domains mediating synapsin I interactions. *J Neurochem* 73:418–428
- Deen AJ, Rilla K, Oikari S, Karna R, Bart G, Hayrinen J, Bathina AR, Ropponen A, Makkonen K, Tammi RH, Tammi MI (2014) Rab10-mediated endocytosis of the hyaluronan synthase HAS3 regulates hyaluronan synthesis and cell adhesion to collagen. *J Biol Chem* 289:8375–8389
- Evanko SP, Potter-Perigo S, Bollyky PL, Nepom GT, Wight TN (2012) Hyaluronan and versican in the control of human T-lymphocyte adhesion and migration. *Matrix Biol* 31:90–100
- Geng F, Zhu W, Anderson RA, Leber B, Andrews DW (2012) Multiple post-translational modifications regulate E-cadherin transport during apoptosis. *J Cell Sci* 125:2615–2625
- Hart GW, Housley MP, Slawson C (2007) Cycling of O-linked beta-*N*-acetylglucosamine on nucleocytoplasmic proteins. *Nature* 446:1017–1022
- Hascall VC, Wang A, Tammi M, Oikari S, Tammi R, Passi A, Vigetti D, Hanson RW, Hart GW (2014) The dynamic metabolism of hyaluronan regulates the cytosolic concentration of UDP-GlcNAc. *Matrix Biol* 35:14–17
- Heldin P, Basu K, Olofsson B, Porsch H, Kozlova I, Kahata K (2013) Deregulation of hyaluronan synthesis, degradation and binding promotes breast cancer. *J Biochem* 154:395–408
- Hiltunen EL, Anttila M, Kultti A, Ropponen K, Penttinen J, Yliskoski M, Kuronen AT, Juhola M, Tammi R, Tammi M, Kosma VM (2002) Elevated hyaluronan concentration without hyaluronidase activation in malignant epithelial ovarian tumors. *Cancer Res* 62:6410–6413
- Hubbard C, McNamara JT, Azumaya C, Patel MS, Zimmer J (2012) The hyaluronan synthase catalyzes the synthesis and membrane translocation of hyaluronan. *J Mol Biol* 418:21–31
- Itano N, Sawai T, Yoshida M, Lenas P, Yamada Y, Imagawa M, Shinomura T, Hamaguchi M, Yoshida Y, Ohnuki Y, Miyauchi S, Spicer AP, McDonald JA, Kimata K (1999) Three isoforms of mammalian hyaluronan synthases have distinct enzymatic properties. *J Biol Chem* 274:25085–25092
- Jiang D, Liang J, Noble PW (2011) Hyaluronan as an immune regulator in human diseases. *Physiol Rev* 91:221–264
- Jokela T, Oikari S, Takabe P, Rilla K, Karna R, Tammi M, Tammi R (2015) Interleukin-1beta-induced reduction of CD44 Ser-325 phosphorylation in human epidermal keratinocytes promotes CD44 homomeric complexes, binding to ezrin, and extended, monocyte-adhesive hyaluronan coats. *J Biol Chem* 290:12379–12393
- Jokela TA, Jauhiainen M, Auriola S, Kauhanen M, Tiihonen R, Tammi MI, Tammi RH (2008) Mannose inhibits hyaluronan synthesis by down-regulation of the cellular pool of UDP-*N*-acetylhexosamines. *J Biol Chem* 283:7666–7673
- Jokela TA, Makkonen KM, Oikari S, Karna R, Koli E, Hart GW, Tammi RH, Carlberg C, Tammi MI (2011) Cellular content of UDP-*N*-acetylhexosamines controls hyaluronan synthase 2 expression and correlates with O-linked *N*-acetylglucosamine modification of transcription factors YY1 and SP1. *J Biol Chem* 286:33632–33640
- Kakizaki I, Kojima K, Takagaki K, Endo M, Kannagi R, Ito M, Maruo Y, Sato H, Yasuda T, Mita S, Kimata K, Itano N (2004) A novel mechanism for the inhibition of hyaluronan biosynthesis by 4-methylumbelliferone. *J Biol Chem* 279:33281–33289
- Karjalainen JM, Tammi RH, Tammi MI, Eskelinen MJ, Agren UM, Parkkinen JJ, Alhava EM, Kosma VM (2000) Reduced level of CD44 and hyaluronan associated with unfavorable prognosis in clinical stage I cutaneous melanoma. *Am J Pathol* 157:957–965
- Kultti A, Pasonen-Seppanen S, Jauhiainen M, Rilla KJ, Karna R, Pyoria E, Tammi RH, Tammi MI (2009) 4-Methylumbelliferone inhibits hyaluronan synthesis by depletion of cellular UDP-glucuronic acid and downregulation of hyaluronan synthase 2 and 3. *Exp Cell Res* 315:1914–1923
- Kultti A, Zhao C, Singha NC, Zimmerman S, Osgood RJ, Symons R, Jiang P, Li X, Thompson CB, Infante JR, Jacobetz MA, Tuveson DA, Frost GI, Shepard HM, Huang Z (2014) Accumulation of extracellular hyaluronan by hyaluronan synthase 3 promotes tumor growth and modulates the pancreatic cancer microenvironment. *Biomed Res Int* 2014:817613
- Manderson AP, Kay JG, Hammond LA, Brown DL, Stow JL (2007) Subcompartments of the macrophage recycling endosome direct the differential secretion of IL-6 and TNFalpha. *J Cell Biol* 178:57–69
- Misra S, Hascall VC, Markwald RR, Ghatak S (2015) Interactions between hyaluronan and its receptors (CD44, RHAMM) regulate the activities of inflammation and cancer. *Front Immunol* 6:201
- Murray RZ, Kay JG, Sangermani DG, Stow JL (2005) A role for the phagosome in cytokine secretion. *Science* 310:1492–1495
- Nakamura Y, Morishita R, Higaki J, Kida I, Aoki M, Moriguchi A, Yamada K, Hayashi S, Yo Y, Matsumoto K (1995) Expression of local hepatocyte growth factor system in vascular tissues. *Biochem Biophys Res Commun* 215:483–488
- Nykopp TK, Rilla K, Sironen R, Tammi MI, Tammi RH, Hamalainen K, Heikkinen AM, Komulainen M, Kosma VM, Anttila M (2009) Expression of hyaluronan synthases (HAS1-3) and hyaluronidases (HYAL1-2) in serous ovarian carcinomas: inverse correlation between HYAL1 and hyaluronan content. *BMC Cancer* 9:143
- Nykopp TK, Rilla K, Tammi MI, Tammi RH, Sironen R, Hamalainen K, Kosma VM, Heinonen S, Anttila M (2010) Hyaluronan synthases (HAS1-3) and hyaluronidases (HYAL1-2)

- in the accumulation of hyaluronan in endometrioid endometrial carcinoma. *BMC Cancer* 10:512
31. Oikari S, Venalainen T, Tammi M (2014) Borate-aided anion exchange high-performance liquid chromatography of uridine diphosphate-sugars in brain, heart, adipose and liver tissues. *J Chromatogr A* 1323:82–86
 32. Peinado H, Aleckovic M, Lavotshkin S, Matei I, Costa-Silva B, Moreno-Bueno G, Hergueta-Redondo M, Williams C, Garcia-Santos G, Ghajar C, Nitadori-Hoshino A, Hoffman C, Badal K, Garcia BA, Callahan MK, Yuan J, Martins VR, Skog J, Kaplan RN, Brady MS et al (2012) Melanoma exosomes educate bone marrow progenitor cells toward a pro-metastatic phenotype through MET. *Nat Med* 18:883–891
 33. Rilla K, Oikari S, Jokela TA, Hyttinen JM, Karna R, Tammi RH, Tammi MI (2013) Hyaluronan synthase 1 (HAS1) requires higher cellular UDP-GlcNAc concentration than HAS2 and HAS3. *J Biol Chem* 288:5973–5983
 34. Rilla K, Pasonen-Seppanen S, Deen AJ, Koistinen VV, Wojciechowski S, Oikari S, Karna R, Bart G, Torronen K, Tammi RH, Tammi MI (2013) Hyaluronan production enhances shedding of plasma membrane-derived microvesicles. *Exp Cell Res* 319:2006–2018
 35. Rilla K, Pasonen-Seppanen S, Karna R, Karjalainen HM, Torronen K, Koistinen V, Tammi MI, Tammi RH, Teravainen T, Manninen A (2012) HAS3-induced accumulation of hyaluronan in 3D MDCK cultures results in mitotic spindle misorientation and disturbed organization of epithelium. *Histochem Cell Biol* 137:153–164
 36. Rilla K, Siiskonen H, Spicer AP, Hyttinen JM, Tammi MI, Tammi RH (2005) Plasma membrane residence of hyaluronan synthase is coupled to its enzymatic activity. *J Biol Chem* 280:31890–31897
 37. Russell DL, Salustri A (2006) Extracellular matrix of the cumulus-oocyte complex. *Semin Reprod Med* 24:217–227
 38. Schmaus A, Klusmeier S, Rothley M, Dimmler A, Sipos B, Faller G, Thiele W, Allgayer H, Hohenberger P, Post S, Sleeman JP (2014) Accumulation of small hyaluronan oligosaccharides in tumour interstitial fluid correlates with lymphatic invasion and lymph node metastasis. *Br J Cancer* 111:559–567
 39. Siiskonen H, Poukka M, Tyynela-Korhonen K, Sironen R, Pasonen-Seppanen S (2013) Inverse expression of hyaluronidase 2 and hyaluronan synthases 1–3 is associated with reduced hyaluronan content in malignant cutaneous melanoma. *BMC Cancer* 13:181
 40. Singleton PA (2014) Hyaluronan regulation of endothelial barrier function in cancer. *Adv Cancer Res* 123:191–209
 41. Sironen RK, Tammi M, Tammi R, Auvinen PK, Anttila M, Kosma VM (2011) Hyaluronan in human malignancies. *Exp Cell Res* 317:383–391
 42. Stern R (2008) Hyaluronan in cancer biology. *Semin Cancer Biol* 18:237
 43. Stern R (2005) Hyaluronan metabolism: a major paradox in cancer biology. *Pathol Biol (Paris)* 53:372–382
 44. Sun J, Lu F, He H, Shen J, Messina J, Mathew R, Wang D, Sarnaik AA, Chang WC, Kim M, Cheng H, Yang S (2014) STIM1- and Orai1-mediated Ca²⁺ oscillation orchestrates invadopodium formation and melanoma invasion. *J Cell Biol* 207:535–548
 45. Takabe P, Bart G, Ropponen A, Rilla K, Tammi M, Tammi R, Pasonen-Seppänen S (2015) Hyaluronan synthase 3 (HAS3) overexpression downregulates MV3 melanoma cell proliferation, migration and adhesion. *Exp Cell Res* 337:1–15. doi:10.1016/j.yexcr.2015.07.026
 46. Tammi RH, Kultti A, Kosma VM, Pirinen R, Auvinen P, Tammi MI (2008) Hyaluronan in human tumors: pathobiological and prognostic messages from cell-associated and stromal hyaluronan. *Semin Cancer Biol* 18:288–295
 47. Tammi RH, Passi AG, Rilla K, Karousou E, Vigetti D, Makkonen K, Tammi MI (2011) Transcriptional and post-translational regulation of hyaluronan synthesis. *FEBS J* 278:1419–1428
 48. Tian X, Azpurua J, Hine C, Vaidya A, Myakishev-Rempel M, Ablaeva J, Mao Z, Nevo E, Gorbunova V, Seluanov A (2013) High-molecular-mass hyaluronan mediates the cancer resistance of the naked mole rat. *Nature* 499:346–349
 49. Toole BP (2009) Hyaluronan-CD44 interactions in cancer: paradoxes and possibilities. *Clin Cancer Res* 15:7462–7468
 50. Toole BP (2004) Hyaluronan: from extracellular glue to pericellular cue. *Nat Rev Cancer* 4:528–539
 51. Toole BP, Slomiany MG (2008) Hyaluronan: a constitutive regulator of chemoresistance and malignancy in cancer cells. *Semin Cancer Biol* 18:244–250
 52. Twarock S, Tammi MI, Savani RC, Fischer JW (2010) Hyaluronan stabilizes focal adhesions, filopodia, and the proliferative phenotype in esophageal squamous carcinoma cells. *J Biol Chem* 285:23276–23284
 53. Vigetti D, Deleonibus S, Moretto P, Bowen T, Fischer JW, Grandoch M, Oberhuber A, Love DC, Hanover JA, Cinquetti R, Karousou E, Viola M, D'Angelo ML, Hascall VC, De Luca G, Passi A (2014) Natural antisense transcript for hyaluronan synthase 2 (HAS2-AS1) induces transcription of HAS2 via protein O-GlcNAcylation. *J Biol Chem* 289:28816–28826
 54. Vigetti D, Deleonibus S, Moretto P, Karousou E, Viola M, Bartolini B, Hascall VC, Tammi M, De Luca G, Passi A (2012) Role of UDP-N-acetylglucosamine (GlcNAc) and O-GlcNAcylation of hyaluronan synthase 2 in the control of chondroitin sulfate and hyaluronan synthesis. *J Biol Chem* 287:35544–35555
 55. Vigetti D, Rizzi M, Moretto P, Deleonibus S, Dreyfuss JM, Karousou E, Viola M, Clerici M, Hascall VC, Ramoni MF, De Luca G, Passi A (2011) Glycosaminoglycans and glucose prevent apoptosis in 4-methylumbelliferone-treated human aortic smooth muscle cells. *J Biol Chem* 286:34497–34503
 56. Warburg O, Posener K, Negelein E (1924) Über den Stoffwechsel der Carcinomzelle. *Biochem Z* 152:309–344
 57. Weigel PH, DeAngelis PL (2007) Hyaluronan synthases: a decade-plus of novel glycosyltransferases. *J Biol Chem* 282:36777–36781
 58. Wu M, Cao M, He Y, Liu Y, Yang C, Du Y, Wang W, Gao F (2015) A novel role of low molecular weight hyaluronan in breast cancer metastasis. *FASEB J* 29:1290–1298
 59. Yang L, Wu XH, Wang D, Luo CL, Chen LX (2013) Bladder cancer cell-derived exosomes inhibit tumor cell apoptosis and induce cell proliferation in vitro. *Mol Med Rep* 8:1272–1278
 60. Zhu W, Leber B, Andrews DW (2001) Cytoplasmic O-glycosylation prevents cell surface transport of E-cadherin during apoptosis. *EMBO J* 20:5999–6007